LETTER

Mitochondrial DNA that escapes from autophagy causes inflammation and heart failure

Takafumi Oka[1], Shungo Hikoso[1], Osamu Yamaguchi[1], Manabu Taneike[1,2], Toshihiro Takeda[1], Takahito Tamai[1], Jota Oyabu[1], Tomokazu Murakawa[1], Hiroyuki Nakayama[3], Kazuhiko Nishida[1,2], Shizuo Akira[4,5], Akitsugu Yamamoto[6], Issei Komuro[1] & Kinya Otsu[1,2]

Heart failure is a leading cause of morbidity and mortality in industrialized countries. Although infection with microorganisms is not involved in the development of heart failure in most cases, inflammation has been implicated in the pathogenesis of heart failure[1]. However, the mechanisms responsible for initiating and integrating inflammatory responses within the heart remain poorly defined. Mitochondria are evolutionary endosymbionts derived from bacteria and contain DNA similar to bacterial DNA[2–4]. Mitochondria damaged by external haemodynamic stress are degraded by the autophagy/lysosome system in cardiomyocytes[5]. Here we show that mitochondrial DNA that escapes from autophagy cell-autonomously leads to Toll-like receptor (TLR) 9-mediated inflammatory responses in cardiomyocytes and is capable of inducing myocarditis and dilated cardiomyopathy. Cardiac-specific deletion of lysosomal deoxyribonuclease (DNase) II showed no cardiac phenotypes under baseline conditions, but increased mortality and caused severe myocarditis and dilated cardiomyopathy 10 days after treatment with pressure overload. Early in the pathogenesis, DNase II-deficient hearts showed infiltration of inflammatory cells and increased messenger RNA expression of inflammatory cytokines, with accumulation of mitochondrial DNA deposits in autolysosomes in the myocardium. Administration of inhibitory oligodeoxynucleotides against TLR9, which is known to be activated by bacterial DNA[6], or ablation of *Tlr9* attenuated the development of cardiomyopathy in DNase II-deficient mice. Furthermore, *Tlr9* ablation improved pressure overload-induced cardiac dysfunction and inflammation even in mice with wild-type *Dnase2a* alleles. These data provide new perspectives on the mechanism of genesis of chronic inflammation in failing hearts.

Mitochondrial DNA has similarities to bacterial DNA, which contains inflammatogenic unmethylated CpG motifs[2–4,7,8]. Damaged mitochondria are degraded by autophagy, which involves the sequestration of cytoplasmic contents in a double-membraned vacuole, the autophagosome and the fusion of the autophagosome with the lysosome[9]. Pressure overload induces the impairment of mitochondrial cristae morphology and functions in the heart[10,11]. We have previously reported that autophagy is an adaptive mechanism to protect the heart from haemodynamic stress[5].

DNase II, encoded by *Dnase2a*, is an acid DNase found in the lysosome[12]. DNase II in macrophages has an essential role in the degradation of the DNA of apoptotic cells after macrophages engulf them[13]. In the present study, we hypothesized that DNase II in cardiomyocytes digests mitochondrial DNA in the autophagy system to protect the heart from inflammation in response to haemodynamic stress.

First, we examined the alteration of DNase II activity in the heart in response to pressure overload. In wild-type mice, pressure overload by

thoracic transverse aortic constriction (TAC) induced cardiac hypertrophy 1 week after TAC and heart failure 8–10 weeks after TAC[5]. DNase II activity was upregulated in hypertrophied hearts, but not in failing hearts (Supplementary Fig. 1a). Immunohistochemical analysis showed infiltration of CD45^{+} leukocytes, including CD68^{+} macrophages in failing hearts (Supplementary Fig. 1b). Then, we stained the heart sections with PicoGreen[14], anti-LAMP2a and anti-LC3 (ref. 15) antibodies, which was used for the detection of DNA, lysosomes and autophagosomes, respectively (Supplementary Figs 1c, d and 2a). We observed PicoGreen- and LAMP2a-positive deposits and PicoGreen- and LC3-positive deposits in failing hearts, but not in hypertrophied hearts, suggesting the accumulation of DNA in autolysosomes in failing hearts.

We crossed mice bearing a *Dnase2a*[flox] allele[13] with transgenic mice expressing Cre recombinase under the control of the α-myosin heavy chain promoter (α-MyHC)[16], to produce *Dnase2a*[flox/flox];α-MyHC-Cre[+] (*Dnase2a*^{−/−}) mice. We used *Dnase2a*[flox/flox];α-MyHC-Cre[−] littermates (*Dnase2a*^{+/+}) as controls. The resulting *Dnase2a*^{−/−} mice were born at the expected Mendelian frequency. In *Dnase2a*^{−/−} mice, we observed a 90.1% reduction in the level of *Dnase2a* messenger RNA (mRNA) and a 95.1% decrease in DNase II activity in purified adult cardiomyocyte preparation (Supplementary Fig. 3a, b). Physiological parameters and basal cardiac function assessed by echocardiography showed no differences between *Dnase2a*^{+/+} and *Dnase2a*^{−/−} mice (Supplementary Table 1). These results indicate that DNase II does not appear to be required during normal embryonic development or for normal heart growth in the postnatal period.

To clarify the role of DNase II in cardiac remodelling, *Dnase2a*^{−/−} mice were subjected to TAC. DNase II activity was upregulated in response to pressure overload in *Dnase2a*^{+/+} hearts and was lower in sham- and TAC-operated *Dnase2a*^{−/−} hearts than that in the corresponding controls (Supplementary Fig. 3c). Twenty-eight days after TAC, 57.1% of *Dnase2a*^{−/−} mice had died, whereas 85.7% of *Dnase2a*^{+/+} mice were still alive (Fig. 1a). The *Dnase2a*^{−/−} hearts showed left ventricular dilatation and severe contractile dysfunction 10 days after TAC (Fig. 1b–d and Supplementary Table 2). The lung-to-body weight ratio, an index of lung congestion, was elevated in TAC-operated *Dnase2a*^{−/−} mice (Fig. 1e). The increases in the heart-to-body weight ratio and cardiomyocyte cross-sectional area by TAC were larger in *Dnase2a*^{−/−} mice than in *Dnase2a*^{+/+} mice (Fig. 1e, f). TAC-operated *Dnase2a*^{−/−} hearts showed massive cell infiltration (Fig. 1f). Immunohistochemical analysis of the hearts showed infiltration of CD45^{+} leukocytes, including CD68^{+} macrophages (Supplementary Fig. 4a). The mRNA level of interleukin (IL)-6 (*Il6*) was upregulated, but not other cytokine mRNAs in TAC-operated *Dnase2a*^{−/−} hearts (Supplementary Fig. 4b). TAC-operated *Dnase2a*^{−/−} hearts showed intermuscular and perivascular fibrosis with increased

[1]Department of Cardiovascular Medicine, Osaka University Graduate School of Medicine, Suita, Osaka 565-0871, Japan. [2]Cardiovascular Division, King's College London, London SE5 9NU, UK. [3]Department of Clinical Pharmacology and Pharmacogenomics, Graduate School of Pharmaceutical Sciences, Osaka University, Suita, Osaka 565-0871, Japan. [4]Laboratory of Host Defense, WPI Immunology Frontier Research Center, Osaka University, Suita, Osaka 565-0871, Japan. [5]Department of Host Defense, Research Institute for Microbial Diseases, Osaka University, Suita, Osaka 565-0871, Japan. [6]Faculty of Bioscience, Nagahama Institute of Bio-Science and Technology, Nagahama, Shiga 526-0829, Japan.
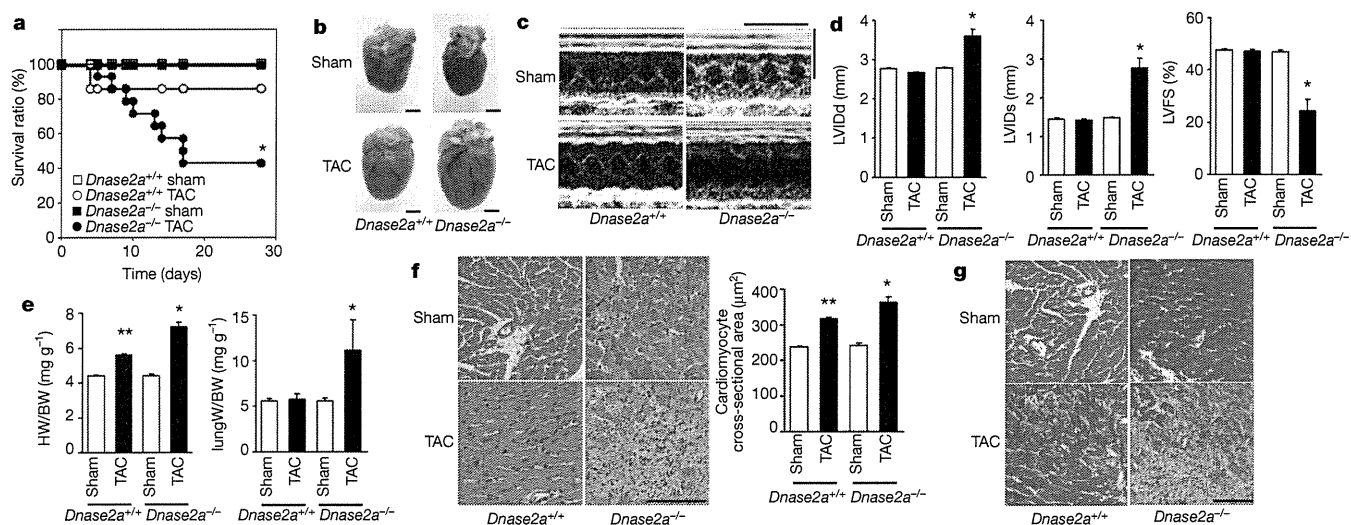
Figure 1 | TAC-induced cardiomyopathy in Dnase2a⁻/⁻ mice. a, Survival ratio after TAC (n = 7–14 per group). **b–g,** Ten days after TAC. **b,** Gross appearance of hearts. Scale bar, 2 mm. **c,** Echocardiography. Scale bars, 0.2 s and 5 mm. Echocardiographic (**d**) and physiological (**e**) parameters (n = 7–13 per group). LVIDd and LVIDs, end-diastolic and end-systolic left ventricular internal dimension, respectively; LVFS, left ventricular fractional shortening; HW/BW, heart/body weight. Haematoxylin and eosin-stained (**f**) and azocarmine and aniline blue (AZAN)-Mallory-stained (**g**) heart sections. Scale bar, 100 μm. Data are mean ± s.e.m. *P < 0.05 versus all other groups, **P < 0.05 versus sham-operated controls.

mRNA expression of α2 type I collagen (*Col1a2*) (Fig. 1g and Supplementary Fig. 3d). Ultrastructural analysis of TAC-operated *Dnase2a⁻/⁻* hearts showed a disorganized sarcomere structure, misalignment and aggregation of mitochondria, and aberrant electron-dense structures (Supplementary Fig. 4c). The mRNA levels of atrial natriuretic factor (*Nppa*) and brain natriuretic peptide (*Nppb*) were higher in TAC-operated *Dnase2a⁻/⁻* mice than in TAC-operated *Dnase2a⁺/⁺* mice (Supplementary Fig. 3d). These data suggest that DNase II plays an important role in preventing pressure overload-induced heart failure and myocarditis.

To clarify the molecular mechanisms underlying the cardiac abnormalities observed in *Dnase2a⁻/⁻* mice, we evaluated the phenotypes in the earlier time course after pressure overload. Chamber dilation and cardiac dysfunction developed with time after TAC in *Dnase2a⁻/⁻* mice

(Supplementary Fig. 5a). We chose to perform the analysis 2 days after TAC to minimize the contributions of operation-related events and phenomena secondary to the initial and essential molecular event that induced cardiomyopathy. TAC-operated *Dnase2a⁻/⁻* hearts showed cell infiltration without apparent fibrosis (Fig. 2a, b) and infiltration of CD68⁺ macrophages and Ly6G⁺ cells (Fig. 2c). We detected increases in the mRNA levels of IL-1β (*Il1b*) and *Il6*, but not interferon-β (*Ifnb1*) and -γ (*Ifng*) or tumour-necrosis factor (TNF)-α in TAC-operated *Dnase2a⁻/⁻* hearts (Supplementary Fig. 6a). To identify the source of IL-1β and IL-6, we performed *in situ* hybridization analysis in heart sections. *Il1b* and *Il6* mRNA-positive cardiomyocytes were evident in TAC-operated *Dnase2a⁻/⁻* hearts (Supplementary Fig. 4d).

Ultrastructural analysis showed aberrant electron-dense deposits without apparent changes in sarcomeric and mitochondrial structures
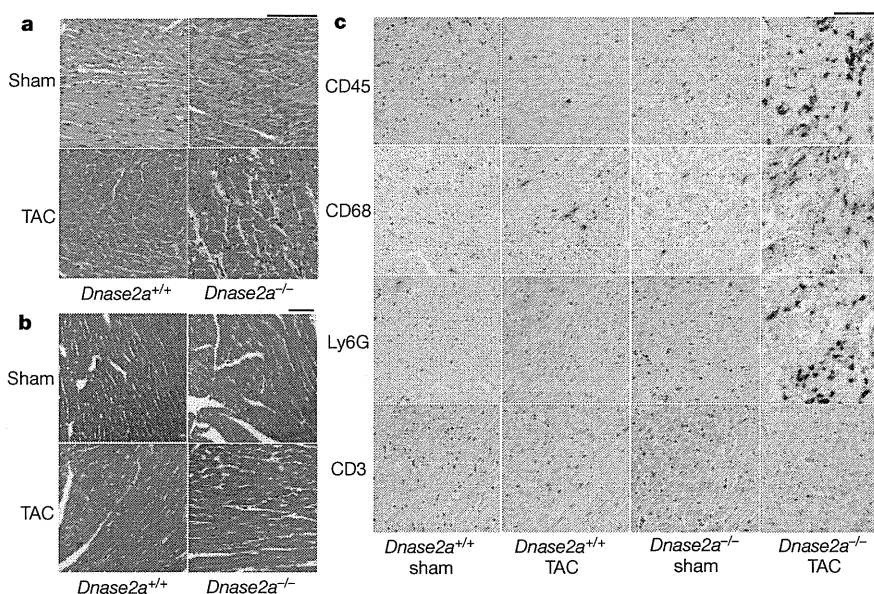

Figure 2 | Pressure overload-induced inflammatory responses in *Dnase2a⁻/⁻* mice 2 days after TAC. Mice were analysed 2 days after TAC (a–c). **a,** Haematoxylin and eosin-stained heart sections. Scale bar, 100 μm.

b, AZAN-Mallory-stained sections. Scale bar, 100 μm.
c, Immunohistochemical analysis using antibodies to CD45, CD68, Ly6G and CD3. Scale bar, 100 μm.

in TAC-operated $Dnase2a^{-/-}$ hearts (Fig. 3a). At higher magnification, the electron-dense deposits appeared to be autolysosomes (Fig. 3a). Immunoelectron microscopic analysis using anti-DNA antibody showed DNA deposition in autolysosomes (Fig. 3b). In TAC-operated $Dnase2a^{-/-}$ hearts, we observed PicoGreen- and LAMP2a-positive deposits and PicoGreen- and LC3-positive deposits (Supplementary Figs 2b and 6b, c). The PicoGreen-positive deposits were not TdT-mediated dUTP nick end labelling (TUNEL)-positive (Supplementary Fig. 6d), indicating that the DNA was not derived from fragmented nuclear DNA. To label mitochondrial DNA, mice were injected with 5-ethynyl-2'-deoxyuridine (EdU) five times before TAC. EdU, a nucleoside analogue to thymidine, is incorporated into DNA during active DNA synthesis[17]. EdU specifically binds to mitochondrial DNA during its active DNA synthesis in non-dividing cardiomyocytes. In TAC-operated $Dnase2a^{-/-}$ hearts, we observed EdU- and LAMP2a-positive deposits and EdU- and LC3-positive deposits (Fig. 3c, d and Supplementary Fig. 2c), indicating that mitochondrial DNA accumulated in autolysosomes.

The innate immune system is the major contributor to acute inflammation induced by microbial infection[18]. TLR9, localized in the endolysosome, senses DNA with unmethylated CpG motifs derived from bacteria and viruses. Mitochondrial DNA activates polymorphonuclear neutrophils through CpG/TLR9 interactions[19]. Immunohistochemical analysis indicated that TLR9 was co-localized with EdU-positive deposits (Fig. 3e). TLR9 is activated by synthetic oligodeoxynucleotides (ODN1668) that contains unmethylated CpG[6], but it is inhibited by inhibitory ligands, such as ODN2088 (ref. 20), in which 'GCGTT' in ODN1668 is replaced with 'GCGGG'. ODN1668 induced increases in $Il1b$ and $Il6$ mRNA levels in wild-type isolated adult cardiomyocytes (data not shown). We, then, examined the effect of ODN2088 on carbonyl cyanide m-chlorophenyl hydrazone (CCCP) or isoproterenol-induced cell death using isolated adult cardiomyocytes to eliminate the contribution of immune cells[5]. CCCP, a protonophore, induces dissipation of mitochondrial membrane potential. Isoproterenol caused a loss of mitochondrial membrane potential in wild-type cardiomyocytes, as indicated by loss of tetramethylrhodamine ethyl ester signal (Supplementary Fig. 7a). Incubation with CCCP or isoproterenol induced conversion of LC3-I to LC3-II, an essential step during autophagosome formation, and treatment with the lysosomal inhibitor bafilomycin A1 led to an even larger increase of LC3-II in CCCP- or isoproterenol-treated cells than in control cells, indicating that CCCP or isoproterenol accelerated autophagic flux (Supplementary Fig. 7b). Isolated cardiomyocytes from $Dnase2a^{-/-}$ hearts were more susceptible than those from control hearts to CCCP or isoproterenol in the presence of
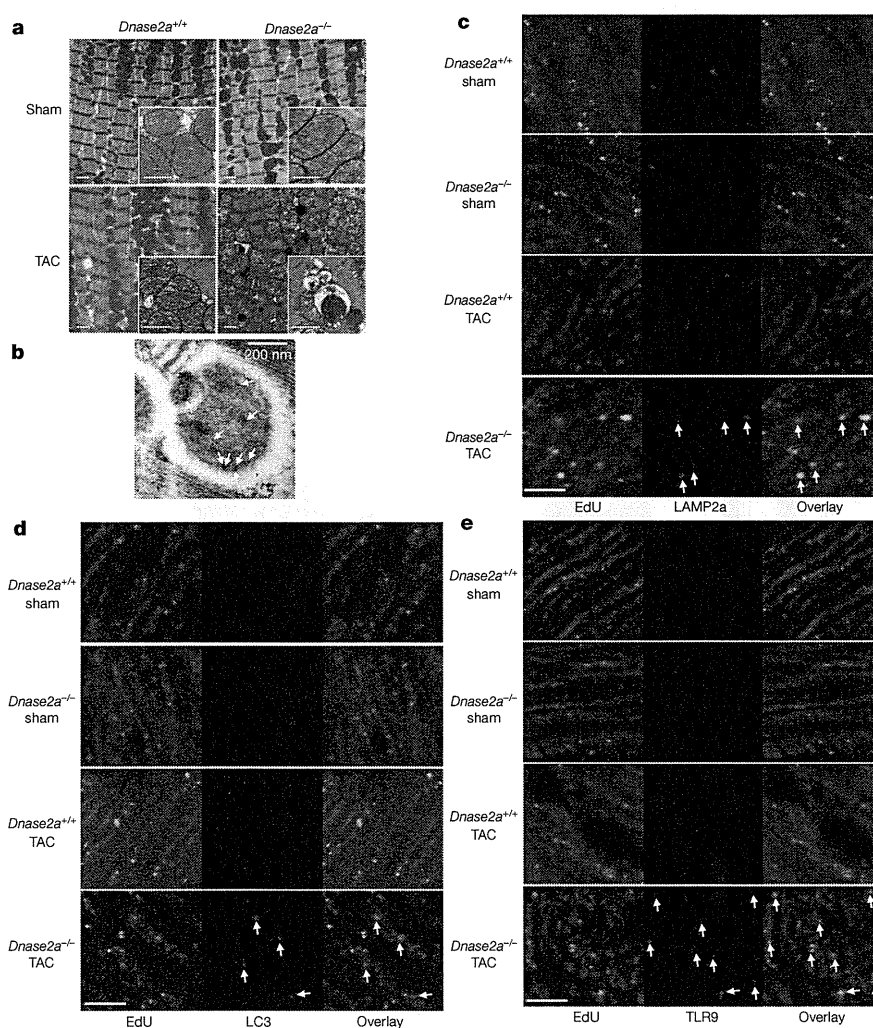

Figure 3 | Deposition of mitochondrial DNA in autolysosomes in pressure-overloaded $Dnase2a^{-/-}$ hearts. Mice were analysed 2 days after TAC (a–e). **a**, Electron microscopic analysis. Images of mitochondria at higher magnification are shown in subsets. Scale bar, 1 µm. **b**, Autolysosome after incubation with anti-DNA antibody and 10 nm gold staining. Scale bar, 200 nm. Arrows indicate labelled DNA. Double staining of heart sections with EdU (green) and anti-LAMP2a antibody (red) (**c**), EdU (green) and anti-LC3 antibody (red) (**d**) or EdU and anti-TLR9 antibody (red) (**e**). Arrows indicate EdU-positive and LAMP2a-, LC3- or TLR9-positive structures. Scale bar, 10 µm.

inactive control oligodeoxynucleotides (ODN2088 control) (Supplementary Fig. 7c–e). CCCP upregulated the mRNA expression levels of *Il1b* and *Il6* in *Dnase2a*$^{-/-}$ cardiomyocytes (Supplementary Fig. 7f). Incubation of *Dnase2a*$^{-/-}$ cardiomyocytes with ODN2088 attenuated the cell death and cytokine mRNA induction by CCCP treatment. Treatment of the *Dnase2a*$^{-/-}$ cardiomyocytes with 3-methyladenine, an autophagy inhibitor, and rapamycin, an autophagy inducer, inhibited and enhanced the induction of the cytokine mRNA by CCCP treatment, respectively (Supplementary Fig. 7g).

We next examined whether the inhibition of TLR9 can rescue the cardiac phenotypes in TAC-operated *Dnase2a*$^{-/-}$ mice. Administration of ODN2088 resulted in the improvement of survival 28 days after TAC (Fig. 4a). ODN2088 attenuated chamber dilation and cardiac dysfunction compared with the control oligodeoxynucleotides 4 days after TAC (Fig. 4b, c and Supplementary Fig. 8a). In addition, ODN2088 inhibited infiltration of CD68$^+$ macrophages and Ly6G$^+$ cells, fibrosis and upregulation of *Il6*, *Ifng*, *Nppa* and *Col1a2* mRNAs in TAC-operated *Dnase2a*$^{-/-}$ hearts (Fig. 4d and Supplementary Fig. 8b–e). ODN2088 prevented cardiac remodelling for a longer time (end-diastolic left ventricular internal dimension (LVIDd), in millimetres, 2.74 ± 0.03, 2.76 ± 0.03; end-systolic left ventricular internal dimension (LVIDs), in millimetres, 1.37 ± 0.03, 1.34 ± 0.05; left ventricular fractional shortening (LVFS) (%), 50.1 ± 0.7, 51.4 ± 1.5, before and 14 days after TAC, respectively, *n* = 6). Furthermore, ablation of *Tlr9* rescued the cardiac phenotypes in TAC-operated *Dnase2a*$^{-/-}$ mice (Supplementary Fig. 9).

To examine the significance of TLR9 signalling pathway in the genesis of heart failure, we subjected TLR9-deficient mice[6] to TAC. Ten weeks after TAC, TLR9-deficient mice showed smaller left ventricular dimensions, better cardiac function and less pulmonary congestion than in TAC-operated control mice (Fig. 4e, f and Supplementary Fig. 10a). The extent of fibrosis, the levels of *Nppa*, *Nppb* and *Col1a2* mRNA, infiltration of CD68$^+$ macrophages were attenuated in TLR9-deficient mice (Supplementary Fig. 10b–e). We detected no significant differences in the cytokine mRNA levels between TAC-operated groups (Supplementary Fig. 10f). Furthermore, ODN2088 improved survival of wild-type mice in a more severe TAC model (Supplementary Fig. 10g). These data indicate that the TLR9 signalling pathway is involved in inflammatory responses in failing hearts in response to pressure overload and plays an important role in the pathogenesis of heart failure.

In this study, we showed that mitochondrial DNA that escapes from autophagy-mediated degradation cell-autonomously leads to TLR9-mediated inflammatory responses in cardiomyocytes, myocarditis and dilated cardiomyopathy. Immune responses are initiated and perpetuated by endogenous molecules released from necrotic cells, in addition to pathogen-associated molecular patterns expressed in invading microorganisms[21]. Cellular disruption by trauma releases mitochondrial molecules, including DNA, into circulation to cause systemic inflammation[19]. Depletion of autophagic proteins promotes cytosolic translocation of mitochondrial DNA and caspase-1-dependent cytokines mediated by the NALP3 inflammasome in response to
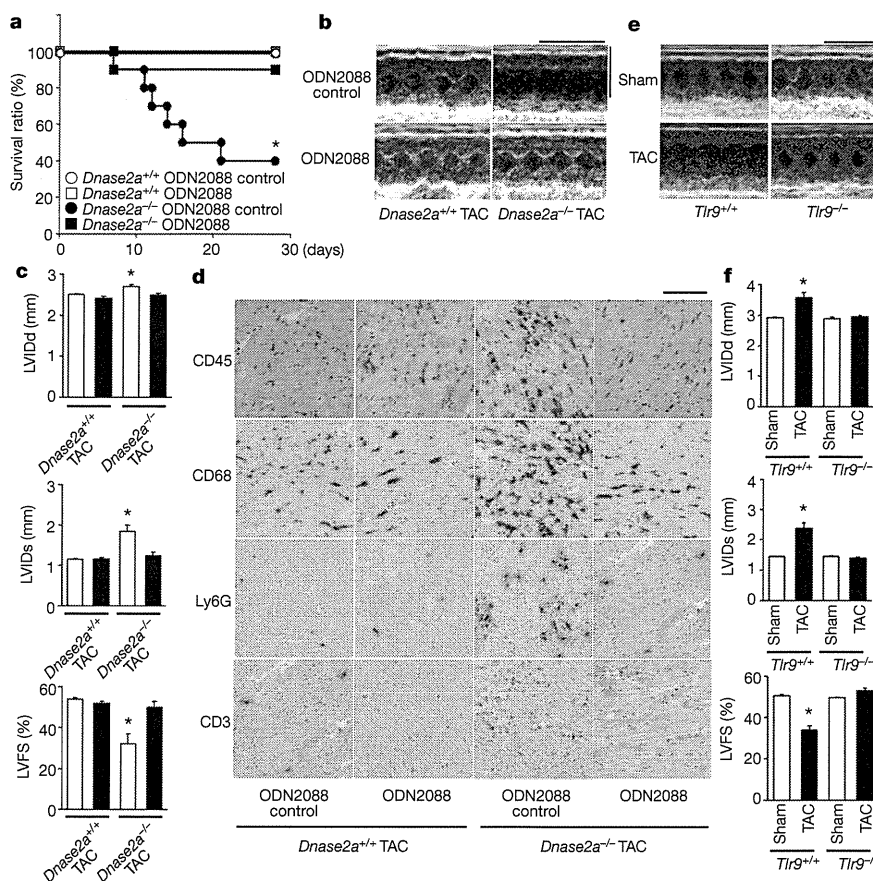

Figure 4 | Inhibition of TLR9 attenuated TAC-induced heart failure.
a, Survival ratio of TAC-operated ODN-treated mice (*n* = 6–10 per group).
b–d, Four days after TAC. b, Echocardiography. Scale bars, 0.2 s and 5 mm.
c, Echocardiographic parameters. Open and closed bars represent ODN2088 control- and ODN2088-treated groups, respectively (*n* = 5–8 per group).

d, Immunohistochemical analysis. Scale bar, 100 μm. TLR9-deficient mice were analysed 10 weeks after TAC (e, f). e, Scale bars, 0.2 s and 5 mm.
f, Echocardiographic parameters (*n* = 6–10 per group). Data are mean ± s.e.m. *P < 0.05 versus all other groups.

lipopolysaccharide in macrophages[22]. We observed no significant difference in the amount of mitochondrial DNA in the blood between TAC-operated $Dnase2a^{-/-}$ and $Dnase2a^{+/+}$ mice (data not shown), excluding a possibility that circulating mitochondrial DNA is causing most of the inflammatory responses mediated by TLR9. The mechanisms presented here do not require release of mitochondrial DNA from cardiomyocytes into extracellular space.

Increased levels of circulating proinflammatory cytokines are associated with disease progression and adverse outcomes in patients with chronic heart failure[1]. Mitochondrial DNA plays an important role in inducing and maintaining inflammation in the heart. This mechanism might work in many chronic non-infectious inflammation-related diseases such as atherosclerosis, metabolic syndrome and diabetes mellitus.

METHODS SUMMARY

Animal study. The study was performed under the supervision of the Animal Research Committee of Osaka University and in accordance with the Japanese Act on Welfare and Management of Animals (No. 105). The 12- to 14-week-old mice were subjected to TAC[5,23] and severe TAC using 26- and 27-gauge needles for aortic constriction, respectively.

Biochemical assays. The DNase II activity was determined by the single radial enzyme-diffusion method[24]. The mRNA levels were determined by quantitative PCR with reverse transcription (RT–PCR)[5].

Histological analysis. The antibodies used were anti-mouse CD45 (ANASPEC), CD68 (Serotec), Ly6G/6C (BD Pharmingen), CD3 (Abcam), DNA (Abcam), LAMP2a (Zymed), LC3 (ref. 25) and TLR9 (Santa-Cruz). The *in situ* hybridization analysis was performed using DIG RNA Labelling Kit and DIG Nucleic Acid Detection Kit (Roche Diagnostics). Hearts were embedded in LR White resin for immunoelectron microscopy[26]. Heart sections were incubated in PicoGreen (Molecular Probes) for 1 h. Twenty-four hours before TAC, mice were injected intraperitoneally with 250 µg of EdU every 2 h five times, and EdU was detected with a Click-iT EdU Alexa Fluor 488 Imaging Kit (Invitrogen).

In vitro and in vivo rescue experiments with the TLR9 inhibitor. Cardiomyocytes[5] were pre-treated with $1\,\mu g\,ml^{-1}$ inhibitory CpG (ODN2088) or control (ODN2088 control) oligodeoxynucleotides for 5 h and incubated with 20 nM CCCP or 50 µM isoproterenol for 24 h (ref. 20). The cells were loaded with tetramethylrhodamine ethyl ester (Molecular Probe) at 10 nM for 30 min. The mice were injected intravenously with 500 µg of the oligodeoxynucleotides 2 h before and 2 and 4 days after TAC, and every 3 days thereafter.

Statistical analysis. Results are shown as the mean ± s.e.m. Paired data were evaluated using a Student's *t*-test. A one-way analysis of variance with the Bonferroni post hoc test was used for multiple comparisons. The Kaplan–Meier method with a log-rank test was used for survival analysis.

Full Methods and any associated references are available in the online version of the paper at www.nature.com/nature.

1. Mann, D. L. Inflammatory mediators and the failing heart: past, present, and the foreseeable future. *Circ. Res.* **91,** 988–998 (2002).
2. Pollack, Y., Kasir, J., Shemer, R., Metzger, S. & Szyf, M. Methylation pattern of mouse mitochondrial DNA. *Nucleic Acids Res.* **12,** 4811–4824 (1984).
3. Cardon, L., Burge, C., Clayton, D. A. & Karlin, S. Pervasive CpG suppression in animal mitochondrial genomes. *Proc. Natl Acad. Sci. USA* **91,** 3799–3803 (1994).
4. Gray, M. W., Burger, G. & Lang, B. F. Mitochondrial evolution. *Science* **283,** 1476–1481 (1999).
5. Nakai, A. *et al.* The role of autophagy in cardiomyocytes in the basal state and in response to hemodynamic stress. *Nature Med.* **13,** 619–624 (2007).
6. Hemmi, H. *et al.* A Toll-like receptor recognizes bacterial DNA. *Nature* **408,** 740–745 (2000).
7. Taanman, J.-W. The mitochondrial genome: structure, transcription, translation and replication. *Biochim Biophys Acta Bioenerget* **1410,** 103–123 (1999).
8. Collins, L., Hajizadeh, S., Holme, E., Jonsso, I. & Tarkowski, A. Endogenously oxidized mitochondrial DNA induces *in vivo* and *in vitro* inflammatory responses. *J. Leukoc. Biol.* **75,** 995–1000 (2004).
9. Mizushima, N., Levine, B., Cuervo, A. M. & Klionsky, D. J. Autophagy fights disease through cellular self-digestion. *Nature* **451,** 1069–1075 (2008).
10. Meerson, F., Zaletayeva, T., Lagutchev, S. & Pshennikova, M. Structure and mass of mitochondria in the process of compensatory hyperfunction and hypertrophy of the heart. *Exp. Cell Res.* **36,** 568–578 (1964).
11. Bugger, H. *et al.* Proteomic remodelling of mitochondrial oxidative pathways in pressure overload-induced heart failure. *Cardiovasc. Res.* **85,** 376–384 (2010).
12. Evans, C. J. & Aguilera, R. J. DNase II: genes, enzymes and function. *Gene* **322,** 1–15 (2003).
13. Kawane, K. *et al.* Chronic polyarthritis caused by mammalian DNA that escapes from degradation in macrophages. *Nature* **443,** 998–1002 (2006).
14. Ashley, N., Harris, D. & Poulton, J. Detection of mitochondrial DNA depletion in living human cells using PicoGreen staining. *Exp. Cell Res.* **303,** 432–446 (2005).
15. Kabeya, Y. *et al.* LC3, a mammalian homologue of yeast Apg8p, is localized in autophagosome membranes after processing. *EMBO J.* **19,** 5720–5728 (2000).
16. Yamaguchi, O. *et al.* Cardiac-specific disruption of the *c-raf-1* gene induces cardiac dysfunction and apoptosis. *J. Clin. Invest.* **114,** 937–943 (2004).
17. Lentz, S. I. *et al.* Mitochondrial DNA (mtDNA) biogenesis: visualization and duel incorporation of BrdU and EdU into newly synthesized mtDNA *in vitro*. *J. Histochem. Cytochem.* **58,** 207–218 (2010).
18. Takeuchi, O. & Akira, S. Pattern recognition receptors and inflammation. *Cell* **140,** 805–820 (2010).
19. Zhang, Q. *et al.* Circulating mitochondrial DAMPs cause inflammatory responses to injury. *Nature* **464,** 104–107 (2010).
20. Stunz, L. *et al.* Inhibitory oligonucleotides specifically block effects of stimulatory CpG oligonucleotides in B cells. *Eur. J. Immunol.* **32,** 1212–1222 (2002).
21. Bianchi, M. E. DAMPs, PAMPs and alarmins: all we need to know about danger. *J. Leukoc. Biol.* **81,** 1–5 (2007).
22. Nakahira, K. *et al.* Autophagy proteins regulate innate immune responses by inhibiting the release of mitochondrial DNA mediated by the NALP3 inflammasome. *Nature Immunol.* **12,** 222–230 (2011).
23. Yamaguchi, O. *et al.* Targeted deletion of apoptosis signal-regulating kinase 1 attenuates left ventricular remodeling. *Proc. Natl Acad. Sci. USA* **100,** 15883–15888 (2003).
24. Koizumi, T. Deoxyribonuclease II (DNase II) activity in mouse tissues and body fluids. *Exp. Anim.* **44,** 169–171 (1995).
25. Lu, Z. *et al.* Participation of autophagy in the degeneration process of rat hepatocytes after transplantation following prolonged cold preservation. *Arch. Histol. Cytol.* **68,** 71–80 (2005).
26. Mosgoller, W. *et al.* Distribution of DNA in human Sertoli cell nucleoli. *J. Histochem. Cytochem.* **41,** 1487–1493 (1993).

Author Contributions S.A. and I.K. provided intellectual input; K.O. was responsible for the overall study design and writing the manuscript. The other authors performed experiments and analysed data. All authors contributed to the discussions.

Author Information Reprints and permissions information is available at www.nature.com/reprints. The authors declare no competing financial interests. Readers are welcome to comment on the online version of this article at www.nature.com/nature. Correspondence and requests for materials should be addressed to K.O. (kinya.otsu@kcl.ac.uk).

METHODS

Animal study. The study was performed under the supervision of the Animal Research Committee of Osaka University and in accordance with the Japanese Act on Welfare and Management of Animals (No. 105).

We crossed mice bearing a $Dnase2a^{flox}$ allele[13] with transgenic mice expressing Cre recombinase under the control of the α-myosin heavy chain promoter (α-MyHC)[16], to produce cardiac-specific DNase II-deficient mice, $Dnase2a^{flox/flox}$;α-MyHC-Cre^{+} ($Dnase2a^{-/-}$). To generate double-knockout mice of $Dnase2a$ and $Tlr9$, we crossed $Dnase2a^{-/-}$ mice with $Tlr9^{-/-}$ mice[6].

The 12- to 14-week-old male mice were subjected to TAC[5,23] and severe TAC using 26- and 27-gauge needles for aortic constriction, respectively. Non-invasive measurements of blood pressure were performed on mice anaesthetized with 2.5% avertin using a blood pressure monitor for rats and mice Model MK-2000 (Muromachi Kikai) according to the manufacturer's instructions[5,23]. To perform echocardiography on awakened mice, ultrasonography (SONOS-5500, equipped with a 15 MHz linear transducer, Philips Medical Systems) was used. The heart was imaged in the two-dimensional parasternal short-axis view, and an M-mode echocardiogram of the midventricle was recorded at the level of the papillary muscles. Heart rate, intraventricular septum and posterior wall thickness, and end-diastolic and end-systolic internal dimensions of the left ventricle were obtained from the M-mode image.

Measurement of DNase II activity. The DNase II activity was determined using the single radial enzyme-diffusion method[24]. The heart homogenates were applied to the cylindrical wells (radius, 1.5 mm) punched in 1% (w/v) agarose gel, containing 0.05 mg ml^{-1} salmon sperm DNA (Type III), 5 μg ml^{-1} ethidium bromide, 0.5 M sodium acetate buffer (pH 4.7) and 10 mM EDTA. After incubation for 48 h at 37 °C, the radius of the dark circle was measured under an ultraviolet transilluminator at 312 nm. DNase II activities for the samples were determined using a standard curve constructed from the serial dilution of porcine DNase II (Sigma).

Quantitative RT–PCR. Total RNA was isolated from the left ventricle or cultured cardiomyocytes for analysis using the TRIzol reagent (Invitrogen Life Technologies). The mRNA levels were determined by quantitative RT–PCR[5]. For reverse transcription and amplification, we used the TaqMan Reverse Transcription Reagents (Applied Biosystems) and Platinum Quantitative PCR SuperMix-UDG (Invitrogen Life Technologies), respectively. The PCR primers and probes were obtained from Applied Biosystems. The primers used were as follows: *Nppa* assay identity, mm01255747_g1; *Nppb* assay identity, mm00435304_g1; *Col1a2* assay identity, Mm01165187_m1; *Gapdh* assay identity, 4352339E; *Il6* assay identity, Mm99999064_m1; *Il1b* assay identity, Mm01336189_m1; *Ifnb1* assay identity, Mm00439546_s1; *Ifng* assay identity,

Mm99999071_m1; *Tnf* assay identity, Mm00443260_g1; and *Dnase2a* assay identity, Mm00438463_m1. We constructed quantitative PCR standard curves using the corresponding complementary DNA, and all data were normalized to *Gapdh* mRNA content.

Histological analysis. Heart samples were excised and immediately fixed in buffered 4% paraformaldehyde, embedded in paraffin and cut into 5 μm sections. Haematoxylin and eosin or AZAN-Mallory staining was performed on serial sections[5,23]. Myocyte cross-sectional area was measured by tracing the outline of 100–200 myocytes in each section[5,23]. For immunohistochemical analysis, frozen heart sections (5 μm) were fixed in buffered 4% paraformaldehyde. The antibodies used were anti-mouse CD45 (ANASPEC), CD68 (Serotec), Ly6G/6C (BD Pharmingen), CD3 (Abcam), LAMP2a (Zymed), LC3 (ref. 25) and TLR9 (Santa-Cruz). For *in situ* hybridization analysis, the mouse IL-6 (1-636) and IL-1β (1-810) RNA probes were labelled using a DIG RNA Labelling Kit and detected using a DIG Nucleic Acid Detection Kit (Roche Diagnostics). For immunoelectron microscopy, frozen heart tissue was embedded in LR White resin and the deposited DNA was detected using anti-DNA antibody (Abcam) and immunogold conjugated anti-mouse IgG (British Biocell International)[26]. For DNA detection, heart sections were incubated in PicoGreen (Molecular Probes) for 1 h. We used EdU to detect mitochondrial DNA in the heart section. Twenty-four hours before TAC, mice were injected intraperitoneally with 250 μg of EdU every 2 h five times, and EdU was detected using a Click-iT EdU Alexa Fluor 488 Imaging Kit (Invitrogen).

***In vitro* and *in vivo* rescue experiments with the TLR9 inhibitor.** Adult mouse cardiomyocytes were isolated from 12- to 14-week-old male mouse hearts as we previously described[5]. Cardiomyocytes were pre-treated with 1 μg ml^{-1} inhibitory CpG oligodeoxynucleotides (ODN2088) (Operon) (5′-TCCTGGCGGGGAA GT-3′) or control oligodeoxynucleotides (ODN2088 control) (5′-TCCTGAGC TTGAAGT-3′) for 5 h and incubated with 20 nM CCCP or 50 μM isoproterenol for 24 h (ref. 20). Cell death was estimated by Trypan blue staining[5]. To monitor mitochondrial membrane potential (Δψ), the cells were loaded with tetramethylrhodamine ethyl ester (Molecular Probes) at 10 nM for 30 min before observation. In *in vivo* study, the mice were injected intravenously with 500 μg of the oligodeoxynucleotides 2 h before and 2 days after TAC, and they were analysed 4 days after TAC. To estimate survival, the mice received additional administration of the oligodeoxynucleotides 4 days after TAC and every 3 days thereafter.

Statistical analysis. Results are shown as the mean ± s.e.m. Paired data were evaluated using a Student's *t*-test. A one-way analysis of variance with the Bonferroni post hoc test was used for multiple comparisons. The Kaplan–Meier method with a log-rank test was used for survival analysis.
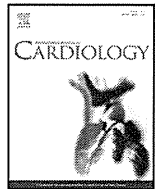
Letter to the Editor

A case of fulminant myocarditis ultimately diagnosed by tenascin C staining

Akihisa Kataoka [a], Hiroyuki Takano [a,*], Taro Imaeda [b], Kwangho Lee [a], Marehiko Ueda [a], Nobusada Funabashi [a], Shigeto Oda [b], Issei Komuro [c], Yoshio Kobayashi [a]

[a] Department of Cardiovascular Science and Medicine, Chiba University Graduate School of Medicine, Chiba, Japan
[b] Department of Emergency and Critical Care Medicine, Chiba University Graduate School of Medicine, Chiba, Japan
[c] Department of Cardiovascular Medicine, Osaka University Graduate School of Medicine, Osaka, Japan

A 20-year-old young male college student, who was previously healthy, suddenly fell down and had a cardiopulmonary arrest in a train on the way to the college. The patient had no previous cardiac symptoms and no family history of cardiac disease or sudden death. A bystander immediately started cardiopulmonary resuscitation on him. Then, an emergency and rescue squad arrived at the scene after 17 minutes and gave him defibrillation shock because the electrocardiographic monitoring showed ventricular fibrillation. The patient was transferred to our hospital with sustained ventricular fibrillation, and finally his sinus rhythm was restored after IABP and PCPS started.

Transthoracic echocardiogram (TTE) on admission demonstrated remarkable LV wall thickening (interventricular septum, 24 mm and LV posterior wall, 22 mm in the parasternal long axis view) and diffuse severe hypokinesis of LV wall motion (LVEF, 10%). The coronary angiogram demonstrated that the coronary arteries were normal (no thrombus and no stenosis) and special laboratory data showed that both anti-β1 adrenoceptor antibody and cardiac-specific autoantibody were negative. On day 4 of hospitalization, he underwent endomyocardial biopsy from LV posterior wall via left femoral artery approach. Histological examination of the specimen with hematoxylin and eosin (HE) revealed no accumulation of inflammatory cells

such as T lymphocytes but extensive interstitial edema was recognized (Fig. 1). These results did not suggest the possibility of active myocarditis. However, immunostaining of TNC could be detected in the interstitial area of biopsy specimens (Fig. 1). The patient was finally diagnosed with fulminant myocarditis with severe myocardial interstitial edema. We started steroid pulse therapy from day 4 of hospitalization for 3 days.

After day 13 of hospitalization, the LVEF gradually increased and the finding of myocardial edema recognized by TTE was improved. And mechanical support devices such as IABP and PCPS could be removed on day 14. On day 55, cardiac MRI was performed. Cardiac MRI revealed delayed enhancement of the endomyocardium of LV, which indicates the presence of myocardial edema in the region (Fig. 2). Thereafter, he continued rehabilitation and finally discharged without severe disorders on day 60.

In the present case, TNC staining was useful to detect myocardial inflammation associate with acute myocarditis. It was reported that all patients with fulminant myocarditis ($n = 11$) had flu-like illness within previous 4 weeks, but our patient had no prior flu-like symptoms. Previous study reported that the clinical assessment of the etiology was inaccurate in 31% of the patients with unexplained cardiomyopathy and that endomyocardial biopsy established the final diagnosis in 75% of these patients with a high degree of specificity [1]. AHA/ACC guidelines state that endomyocardial biopsy should be performed in the setting of unexplained, new-onset heart failure of <2 weeks duration associated with a normal-sized or dilated LV in addition to hemodynamic compromise [2]. Although his clinical presentations were compatible with fulminant myocarditis, HE staining of the endomyocardial biopsy specimens did not demonstrate the findings of active myocarditis which are focal inflammatory infiltrate with adjacent myocytolysis according to the Dallas criteria. The Dallas criteria have been used as the gold standard for the histologic diagnosis of myocarditis despite criticism concerning sampling error and variations in the histologic interpretation by routine staining.

TNC is one of the extracellular matrix glycoproteins and it is sparse in mature tissue but reappears in association with wound healing or cancer invasion [3]. In the heart, TNC is expressed only at the very early stages of embryonic development but reappears in the myocardium under various pathological conditions such as acute myocardial infarction and acute myocarditis [4]. TNC was specifically expressed in myocardium during active stage of myocarditis, and then disappeared in the healing stage of myocarditis in mouse model. During myocarditis, several cytokines including interleukin-1β and tumor

* Corresponding author at: Department of Cardiovascular Science and Medicine, Chiba University Graduate School of Medicine, 1-8-1 Inohana, Chuo-ku, Chiba 260-8670, Japan. Tel.: +81 43 226 2555; fax: +81 43 226 2096.
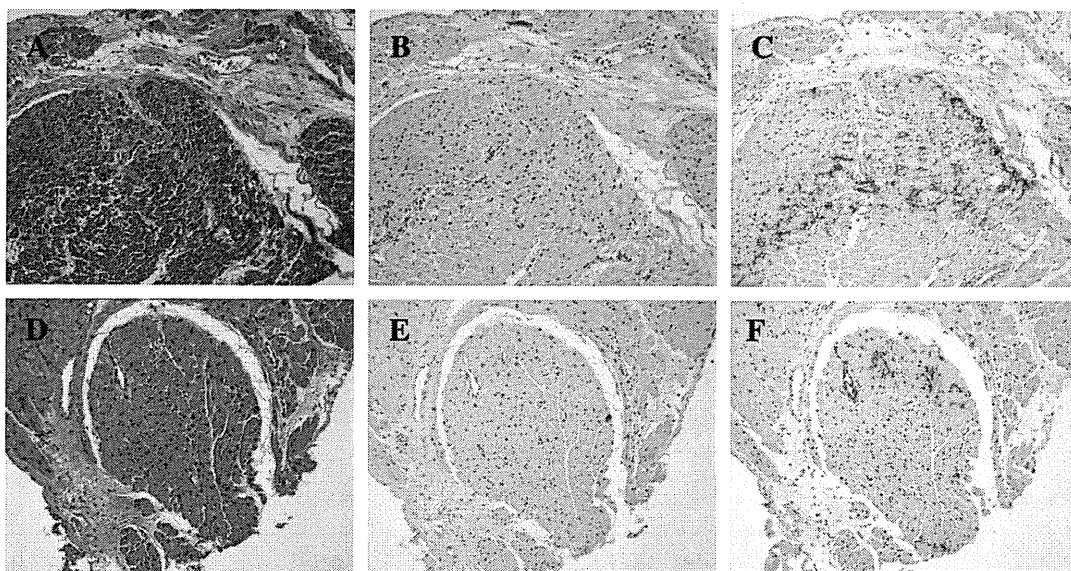E-mail address: htakano-cib@umin.ac.jp (H. Takano).

Fig. 1. Histological results of endomyocardial biopsies from left ventricle. A and D, hematoxylin and eosin staining. B and E, immunostaining for T lymphocytes. C and F, immunostaining for tenascin C.
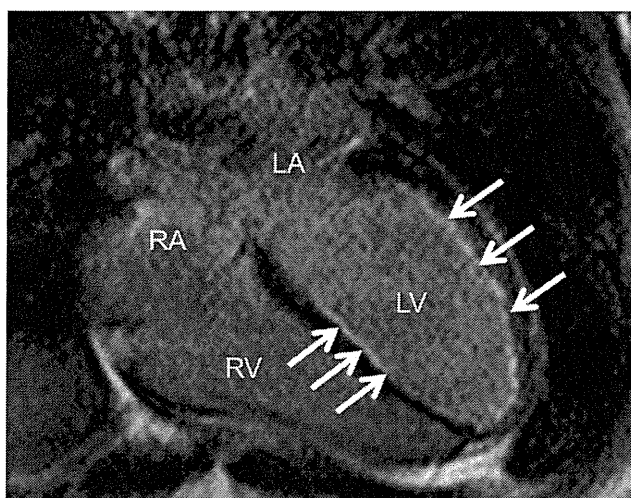

Fig. 2. Four-chamber views of contrast-enhanced cardiac MRI on day of 55 hospitalization. Delayed enhancements (arrows) were observed in part of the endomyocardium. Abbreviations: LA, left atrium; LV, left ventricle; RA, right atrium; RV, right ventricle.

necrosis factor-α are expressed at the early stage and induce the expression of TNC. TNC could be considered a sensitive marker for active inflammation [5]. In the present case, immunostaining for TNC in biopsy specimens was useful for the diagnosis of fulminant myocarditis. Delayed enhanced cardiac MRI imaging, which was performed after attenuation of myocardial edema and stabilization of hemodynamics, also suggested the existence of myocardial inflammation.

The authors of this manuscript have certified that they comply with the Principles of Ethical Publishing in the International Journal of Cardiology (Shewan and Coats 2010;144:1–2).

References

[1] Ardehali H, Qasim A, Cappola T, et al. Endomyocardial biopsy plays a role in diagnosing patients with unexplained cardiomyopathy. Am Heart J 2004;147:919–23.
[2] Cooper LT, Baughman KL, Feldman AM, et al. The role of endomyocardial biopsy in the management of cardiovascular disease: a scientific statement from the American Heart Association, the American College of Cardiology, and the European Society of Cardiology. Circulation 2007;116:2216–33.
[3] Erickson HP. Tenascin-C, tenascin-R and tenascin-X: a family of talented proteins in search of functions. Curr Opin Cell Biol 1993;5:869–76.
[4] Imanaka-Yoshida K, Hiroe M, Yasutomi Y, et al. Tenascin-C is a useful marker for disease activity in myocarditis. J Pathol 2002;197:388–94.
[5] Morimoto S, Imanaka-Yoshida K, Hiramitsu S, et al. Diagnostic utility of tenascin-C for evaluation of the activity of human acute myocarditis. J Pathol 2005;205:460–7.

CARDIOLOGY
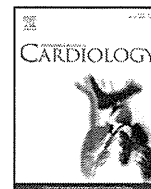
Comparison of image characteristics of plaques in culprit coronary arteries by 64 slice CT and intravascular ultrasound in acute coronary syndromes

Hiroyuki Takaoka [a], Iwao Ishibashi [b], Masae Uehara [a], Geoffrey D. Rubin [c], Issei Komuro [a], Nobusada Funabashi [a,*]

[a] Department of Cardiovascular Science and Medicine, Chiba University Graduate School of Medicine, 1-8-1 Inohana, Chuo-ku, Chiba City, Chiba 260-8670, Japan
[b] Department of Cardiology, Chiba Emergency Medical Center, 3-32-1, Isobe, Mihamaku, Chiba City, Chiba, 261-0012, Japan
[c] Department of Radiology, Stanford University, 1201 Welch Rd, P170, Stanford, CA 94305-5488, USA

ARTICLE INFO

ABSTRACT

Purpose: To evaluate plaque image characteristics in coronary artery culprit-lesions in subjects with acute coronary syndromes (ACS), we retrospectively compared coronary arterial images by 64-slice CT before conventional-coronary-angiogram with those by intravascular ultrasound (IVUS).
Materials-and-methods: Retrospective analysis of coronary arterial images from thirty-one subjects (26-males, mean age 59.3 ± 12.0 years) exhibiting acute symptoms with suspicion of ACS, where either (1) ECG was un-interpretable or (2) ECG was non diagnostic/cardiac biomarkers was equivocal; with significant stenosis on emergent 64 slice CT and subjects were finally diagnosed as having ACS confirmed by conventional-coronary-angiogram, followed by IVUS before coronary-intervention. After principal culprit-lesion components were classified into 1) thrombus, 2) soft plaques, and 3) fibrotic plaques by IVUS, corresponding culprit-lesion CT values were measured (two-observers).
Results: Nineteen and 12 of 31 subjects were finally diagnosed as unstable angina pectoris and non-ST elevation acute myocardial infarction respectively. Main culprit-lesion components of ACS were identified on MSCT in all subjects. Culprit-lesion CT values diagnosed as soft plaques by IVUS (n = 6, 32.9 ± 8.7 HU) were not lower than those of thrombi (n = 18, 43.2 ± 10.7 HU, p = 0.268); both values were significantly lower than those of fibrotic plaques (n = 7, 82.5 ± 22.6 HU) (both p < 0.01). Calcification, spotty calcification, and positive arterial remodeling were observed in 67.7%, 61.3%, 58.1% (IVUS) and 58.1%, 51.6%, 74.2% (MSCT), respectively (all p = NS). CT value reproducibilities and culprit-lesion areas, were 0.87 and 0.86, respectively (two analyzers).
Conclusions: 64-slice CT can non-invasively evaluate image characteristics in coronary artery culprit-lesions in ACS subjects accurately; this may help to differentiate soft plaques or thrombi generated by plaque rupture from fibrotic plaques.

© 2011 Elsevier Ireland Ltd. All rights reserved.

1. Introduction

Evaluation of the characteristics of coronary arterial plaques using intravascular ultrasound (IVUS) has been recognized as useful for evaluating the stability of coronary arterial plaques [1,2]. IVUS-derived image characteristics of plaques in culprit coronary arteries in acute coronary syndromes (ACS) have been recognized as follows 1) low-echoic plaque, 2) spotty calcification and 3) positive arterial remodeling [3].

However, there are few reports in which plaques in culprit coronary arteries in ACS were evaluated by non-invasive diagnostic modalities and compared with evaluation by IVUS. Recently, the utility of 64-slice multislice computed tomography (CT) (MSCT) has been established for evaluating coronary artery disease [4–6] as well

as myocardium [7–9]. There have been several reports in which comparison of coronary arterial images evaluated by MSCT with traditional classification by IVUS showed good correlation [10,11].

In this study, to non-invasively evaluate image characteristics of plaque in culprit lesions in coronary arteries of subjects with ACS, we compared coronary arterial images by 64-slice CT before conventional coronary angiogram (CAG) with those by IVUS following CAG and before coronary intervention.

2. Materials and methods

We retrospectively analyzed coronary arterial images of subjects exhibiting acute symptoms with suspicion of ACS where either (1) the electrocardiogram (ECG) was un-interpretable or (2) non diagnostic ECG or cardiac biomarker results were equivocal; with significant stenosis on emergent 64 slice CT and were finally diagnosed as having ACS confirmed by CAG, followed by IVUS before coronary intervention.

Exclusion criteria for CT examination in this study were as follows: subjects with 1) American Heart Association (AHA) criteria Class 1 for indication of emergency percutaneous coronary intervention including 2) presence of de novo ST elevation in

* Corresponding author. Tel./fax: +81 43 226 2655.
E-mail addresses: funanobu2005@yahoo.co.jp, nobusada@w8.dion.ne.jp (N. Funabashi).

Table 1
Baseline characteristics of all subjects.

N	31
Age (years)	59.3 ± 12.0
Males	26 (83.9%)
Hypertension	21 (67.7%)
Hyperlipidemia	18 (58.1%)
Diabetes mellitus	10 (32.3%)
Smokers	24 (77.4%)
Body mass index	25.0 ± 3.1

the ECG and referral to our Institute within 12 h after onset, or within more than 12 h after onset, but still having continuous chest pain; 3) cardiogenic shock; 4) fatal arrhythmia; 5) renal dysfunction (serum creatinine ≧2.0 mg/dl); and 6) history of allergy to iodinated contrast material. Finally, we retrospectively collected data from 31 subjects (26 males, mean age 59.3 ± 12.0 years) who were eligible under these criteria.

Average times from the onset of symptoms to hospital arrival were 14.4 ± 23.3 h. Baseline characteristics of all subjects are shown in Table 1. All patients provided written informed consents for all procedures in this examination.

2.1. 64-slice CT protocol

All 31 subjects underwent 64-slice CT (Light Speed VCT, GE Healthcare, Milwaukee, WI, USA) before CAG with IVUS. Subjects whose heart rates were more than 60 beats per minute, received 2–8 mg propranolol before the MSCT scan.

Contrast material was administered via a 20-gauge needle into the antecubital vein. Initially, the transit time was measured by injecting 8 ml of contrast material (350 mg/ml iodine concentration, Omnipaque; Daiichi Sankyo Pharmaceutical Co, Ltd, Tokyo, Japan), followed by 20 ml of saline, and by repetitively scanning the ascending aorta at the level of the left main coronary artery; the transit time was determined as the interval from the start of injection to peak enhancement in the ascending aorta. Depending on this time, the total volume of contrast material was determined, ranging from 45 to 63 ml depending on renal function or body weight; this volume was then injected at a rate of 4 ml/s, followed by 47 ml of saline at 3.5 ml/s with a double channel injection system (Dual Shot, Nemoto, Tokyo, Japan).

Retrospective ECG-gated enhanced 64-slice CT was then performed with a slice thickness of 0.625 mm, a gantry rotation speed of 350 ms per rotation, and a tube voltage of 120 kV. The tube current was increased up to 750 milliamperes (mA) only in 35–80% of the R-to-R interval of the ECG, where the motion of the heart and coronary arteries tends to be static.

Conversely, the tube current was decreased to less than 300 mA only in 85–30% of the R-to-R interval, in order to reduce the total radiation exposure. After acquisition, a total of twenty phases during one cardiac cycle (0–95% of the R-to-R interval of the ECG, 5% interval) were extracted and all of the optimal cardiac phase data with the minimum motion artifacts were transferred to a workstation (Virtual place, Aze, Tokyo, Japan).

2.2. Image analysis of coronary arteries by 64-slice CT

We first evaluated the presence of significant stenosis or occlusion of coronary arteries in all 15 segments according to AHA classifications in axial source images and multi and curved planar reformation of long- and short-axis images of coronary arteries in MSCT. If there were 2 or more significant stenotic or occluded lesions, we regarded one of them as the culprit lesion depending on other clinical information, such as the ECG or transthoracic echocardiogram.

Next, consecutive cross-sectional CT images of the vessels perpendicular to the stretched curved planar reformation similar to the IVUS images were created; CT values and area of plaque or thrombi in culprit lesions were measured and presence of calcification, spotty calcification (Fig. 1) and positive arterial remodeling (Fig. 2) in MSCT images was evaluated by two experienced cardiologists (I.I. and H.T.).

The plaque components of the culprit lesions were identified with reference to the corresponding lesion in IVUS images, using the distance from the ostium or some side branches and calcification as landmarks for these locations. The details of definition of plaque components in IVUS are indicated in the IVUS Protocol Section below. If the culprit lesions were occluded, we measured CT values at the proximal portion of the occluded lesion.

2.3. Definition of calcification and arterial remodeling on CT

Calcification in a culprit lesion was defined as a mass whose CT value was more than 130 HU and whose area was more than 1 mm^2 in CT images, according to the definition of Agatston [12]. Among these calcifications, we defined a spotty calcification as a mass whose area was less than 5 mm^2 in CT images [13] (Fig. 1).

The arterial remodeling index (RI) was defined as the ratio of the cross-sectional area (CSA) of the vessel wall at the culprit lesion site to the CSA of the vessel wall at the proximal reference site (Fig. 2).

The definitions of vessel wall, culprit lesions and those areas are different from IVUS, in which the vessel wall was defined as the external elastic membrane (EEM), while the culprit lesions were defined as the site with minimum residential luminal points; if the culprit artery was occluded, the culprit area was measured at the most proximal lesion in occluded lesions.

The presence of positive remodeling was defined in this study as having an RI more than 1.05, using both MSCT and IVUS [3].

2.4. IVUS protocol

After we detected the culprit lesion by CAG, we performed IVUS for accurate evaluation of the culprit lesion and decision on an appropriate strategy. Subjects were classified into those with or without calcification and positive arterial remodeling. IVUS (TU-C200C, Terumo, Tokyo, Japan) was performed with 40 mH using an intrafocus catheter and images were obtained with a 0.5 mm/s auto pullback method before coronary intervention. IVUS was performed on average 31.8 ± 68.1 h after MSCT acquisition. Plaque configurations were classified according to IVUS criteria by two experienced cardiologists (I.I. and H.T.), as recently reported [10]. Briefly, the classification consists of the following three groups: 1) Soft plaque: most of the plaque area is composed of tissue with an echogenicity lower than that of the adventitia (Fig. 3a); 2) Fibrotic plaque: most of the plaque area is composed of tissue producing echoes as bright or brighter than the adventitia but without acoustic shadows (Fig. 3b); and 3) Thrombus: most of the plaque area is composed of thrombus with some mobility. In IVUS images, a thrombus is usually recognized as an intraluminal mass, often with a layered, lobulated, or pedunculated appearance (Fig. 3c) [10,14]. We classified all components on the basis of the above-mentioned three categories, and according to the major components observed among the severest stenotic lesions by IVUS.

2.5. Definition of calcification on IVUS

In each subject, based on the outcome of the quantification of coronary calcium deposits in IVUS images, the culprit lesions were categorized as belonging to one of the following three groups with reference to the definition recently outlined and modified slightly by us: 1) No calcification: a lesion in which calcium is not detected; 2) Spotty calcification: a lesion that contains only small calcium deposits within an arc of less than 90°; and 3) Extensive calcification: extensive calcified lesions with an arc of more than 90° in one or more cross-sectional images of the lesion.
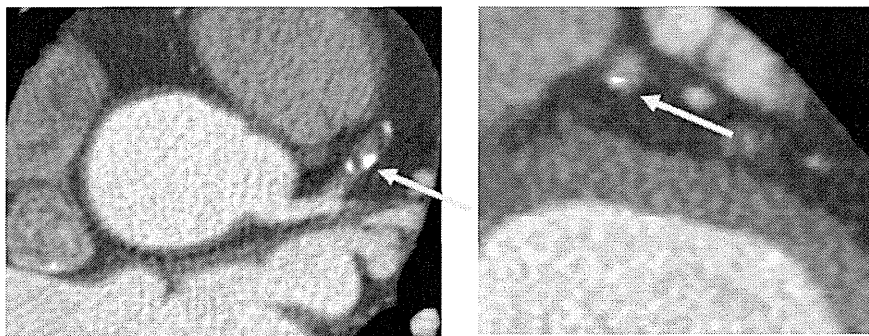

Fig. 1. Typical images of spotty calcification in culprit coronary arteries on multislice computed tomography (CT). Left figure; axial source images of enhanced CT revealed spotty calcification (yellow arrow) in low CT area completely occluding the lumen of left anterior descending branch (LAD). Right figure: multiplanar reformation images of short axis of LAD. Spotty calcification in low CT area completely occluding the lumen of LAD can be observed.
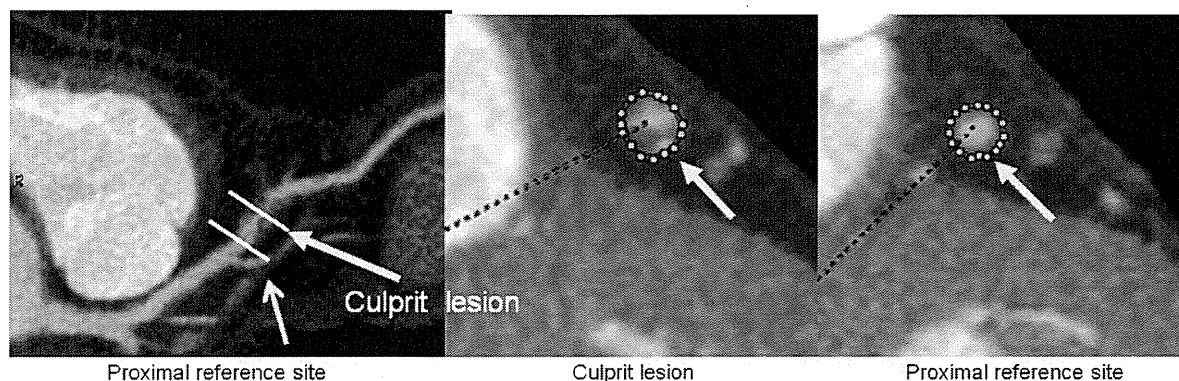
Proximal reference site   Culprit lesion   Proximal reference site

Fig. 2. Definition of remodeling index (culprit area/proximal reference area) in multislice computed tomography (CT). Curved planar reformation images of left anterior descending branch (LAD) (left figure) and short axis images perpendicular to long axis of LAD at 1) culprit lesion (middle figure) and 2) proximal reference site (right figure) made from left figure. Vessel size surrounded by green dots was larger in culprit lesion than in proximal reference site, which suggests presence of positive remodeling. Remodeling index (RI) was defined as the ratio of the cross-sectional area (CSA) of the vessel wall at the culprit lesion site to the CSA of the vessel wall at the proximal reference site. Positive remodeling categories were defined as having a remodeling index more than 1.05, which is the same definition used in a study employing IVUS.

2.6. Statistics

All numeric results are expressed as mean ± standard deviation (SD). Statistical analysis was performed using one-way ANOVA and Tukey's multiple comparison with statistical software SPSS (SPSS Japan Inc, version 17.0, Tokyo, Japan) when comparing CT values among 3 plaque components. Values with $p < 0.05$ were considered statistically significant. We compared the ratio of the presence of coronary calcification to positive remodeling using the chi-square test. We used Pearson's correlation coefficient for assessment of inter-observer variability.

3. Results

Among 31 subjects, 19 subjects were finally diagnosed as unstable angina pectoris and 12 subjects were diagnosed as non-ST elevation acute myocardial infarction. Culprit coronary arteries diagnosed by CAG and IVUS were left anterior descending branch in 18 subjects, left circumflex branch in 8 subjects, right coronary artery in 4 subjects, and high lateral branch in one subject.

Main components of plaque culprit lesions in ACS were diagnosed to be thrombus in 18 subjects, soft plaques in 6 subjects, and fibrotic plaques in 7 subjects by IVUS and were identified by CT in all subjects.

3.1. Comparison of CT values among the three different components of culprit lesions diagnosed by IVUS

Typical images of each type of plaque by IVUS and corresponding MSCT images on CAG are shown in Fig. 3. CT values of culprit lesions diagnosed as soft plaques (n = 6) by IVUS were 32.9 ± 8.7 HU; these values were lower than those of thrombi, but not significantly (n = 18, 43.2 ± 10.7 HU, p = 0.268), while both were significantly lower than those of fibrotic plaques (n = 7, 82.5 ± 22.6 HU) (both, p < 0.01) (Fig. 4).

3.2. Proportion of culprit lesions with calcification and spotty calcification in coronary arteries detected by IVUS and CT

Calcification was observed in 67.7% of culprit lesions in IVUS and 58.1% of culprit lesions in CT and spotty calcification were observed in 61.3% of culprit lesions by IVUS and in 51.6% by CT; furthermore, these proportions were not significantly different between IVUS and CT (p = 0.43 and 0.44, respectively) (Fig. 5).

3.3. Proportion of culprit lesions with positive arterial remodeling in coronary arteries by IVUS and CT

Positive arterial remodeling was observed in 58.1% of culprit lesions in coronary arteries by IVUS and in 74.2% by CT; these proportions were not significantly different between IVUS and CT (both p = 0.18) (Fig. 6).

3.4. Inter-observer variability between two observers of ct values and area of plaque or thrombi in culprit lesions

The correlation coefficient of CT values of plaque or thrombi was 0.87 between two observers (Fig. 7) and the Bland and Altman plot of CT values of plaque or thrombi in culprit lesions revealed a mean difference ± 2SD of 1.5 ± 25.4 HU (Fig. 8).

The correlation coefficient of area of plaque or thrombi in culprit lesions on CT was 0.86 between two observers (Fig. 9) and the Bland and Altman plot of area of plaque or thrombi in culprit lesions revealed a mean difference ± 2SD of 3.3 ± 6.6 mm² (Fig. 10).

3.5. Relationship between area of plaque or thrombi in culprit lesions on CT and those on IVUS

In this analysis, the measurements of areas of plaque or thrombi in culprit lesions on CT were averages of the measurements analyzed by two observers. The correlation coefficient of the areas between CT and IVUS was 0.49 (Fig. 11) and the Bland and Altman plot of area of plaque or thrombi in culprit lesions between CT and IVUS revealed a mean difference ± 2SD of 4.9 ± 11.9 mm²; in addition, CT tended to overestimate the area of plaque or thrombi in culprit lesions in coronary arteries compared with IVUS (Fig. 12).

3.6. Other specific findings indicating vulnerabilities of coronary arterial plaque observed on MSCT only

Recent research has shown that vulnerable plaques tend to have associated vasa vasorum [15]. Ring enhancement signs observed on MSCT only may be a sign of the presence of vasa vasorum in coronary arterial plaques. We found ring enhancement signs in culprit lesions of coronary arteries in 14 subjects (45.2%) in this ACS population.
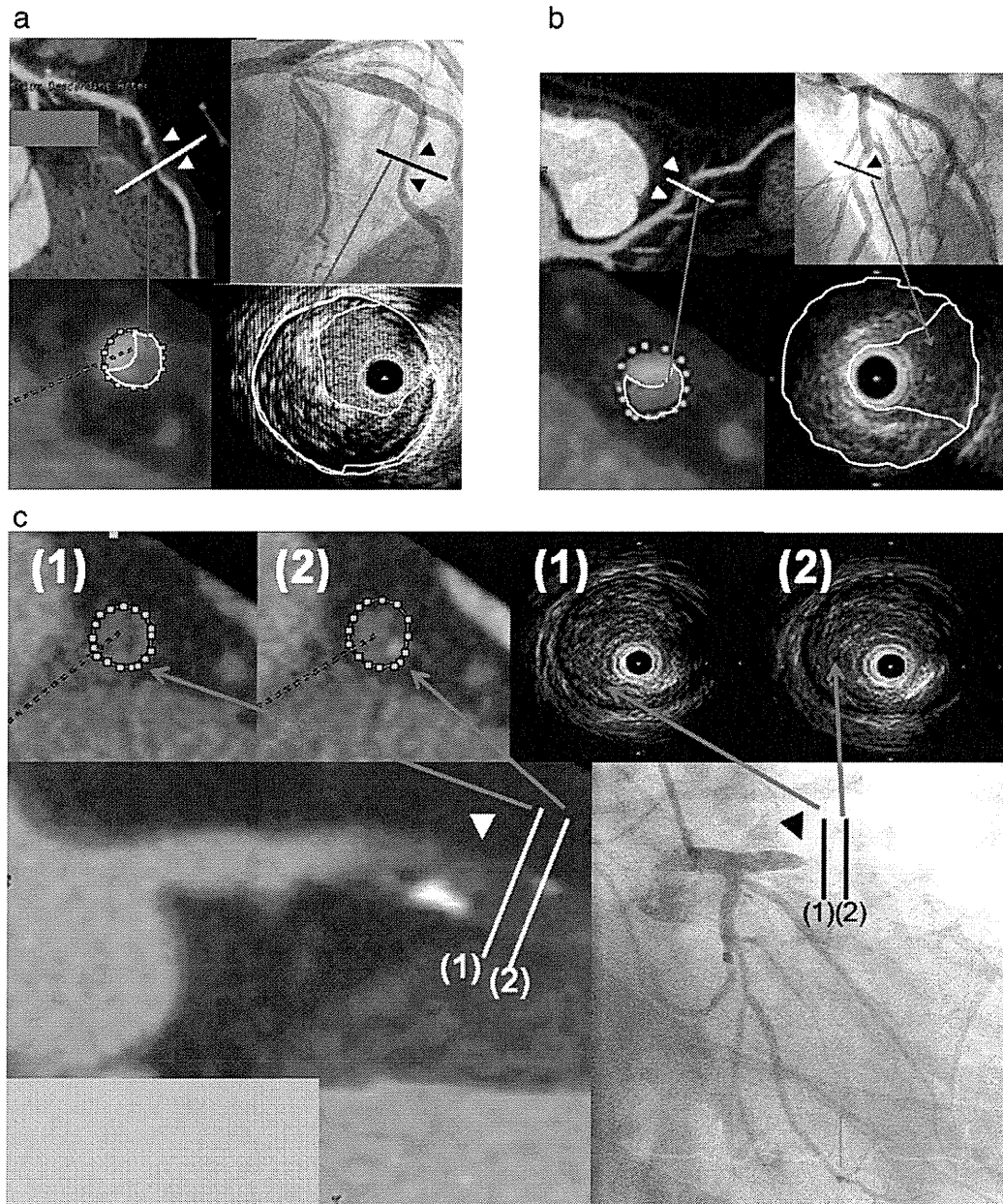
Fig. 3. Typical images of each type of plaque by intravascular ultrasound (IVUS) and corresponding multislice computed tomographic (CT) images with conventional coronary angiogram (CAG). a. Typical CT images (left upper and lower figures) of soft plaques identified by IVUS (right lower figure) acquired from a 76 year old male. Curved planar reformation images of left anterior descending branch (LAD) (left upper figure) revealed significant stenosis with non calcified plaques (white arrow heads) in the middle portion of LAD; short axis images of coronary arteries (left lower figure) were made perpendicular to the long axis of LAD (white bar in left upper figure) in which low CT area (average 36 HU, surrounded by white circle) occupied more than 50% of cross sectional area (CSA) of the coronary arterial lumen (surrounded by green dots). CAG (right upper figure) also revealed significant stenosis in the middle portion of LAD (black arrow heads), and at the corresponding site of the black bar in CAG, soft plaque could be observed in IVUS (right lower figure). Considering the distance from the ostium and presence of the side branch etc. as the landmark of the location of the plaques, we concluded that the soft plaques in IVUS (right lower figure) correspond to the non-calcified plaques in short axis images of coronary arteries in CT (left lower figure). b. Typical CT images (left upper and lower figures) of fibrotic plaques identified by IVUS (right lower figure) acquired from a 41 year old male. Curved planar reformation images of LAD (left upper figure) revealed significant stenosis with non-calcified plaques (white arrow heads) in the middle portion of LAD; short axis images of coronary arteries (left lower figure) were made perpendicular to the long axis of LAD (white bar in left upper figure) in which low CT area (average 88 HU, surrounded by white circle) occupied more than 50% of CSA of coronary arterial lumen surrounded by green dots. CAG (right upper figure) also revealed significant stenosis in the middle portion of LAD (black arrow head) and at the corresponding site of the black bar in CAG, fibrotic plaque can be observed in IVUS (right lower figure). Considering the distance from the ostium and presence of the side branch etc. as the landmark of the location of the plaques, we concluded that the fibrotic plaques in IVUS (right lower figure) correspond to the non-calcified plaques in short axis images of coronary arteries in CT (left lower image). c. Typical images of thrombi by IVUS and corresponding CT images. Thrombi were observed in the proximal LAD in IVUS in a 65 year old male and at the corresponding site in CT.Typical CT images (left figures) of thrombi identified by IVUS (right upper figures) acquired from a 65 year old male. Curved planar reformation images of LAD (left upper figure) revealed complete occlusion with low CT area (white arrow head) with spotty calcified plaques in the proximal portion of LAD; short axis images of coronary arteries (left upper figures) were made perpendicular to the long axis of LAD (white bar (1) and (2) in left lower figure) in which low CT area (average 49 HU) occupied 100% of CSA of coronary arterial lumen surrounded by green dots. CAG (right lower figure) also revealed complete occlusion in proximal portion of LAD (black arrow head) and at the corresponding site of the black bar in CAG, movable thrombi could be observed in IVUS (right upper figures). Considering the distance from the ostium and presence of the side branch etc. as the landmark of the location of the plaques, we concluded that the thrombi in IVUS (right upper figures) correspond to the low CT area in short axis images of coronary arteries in CT (left lower image).
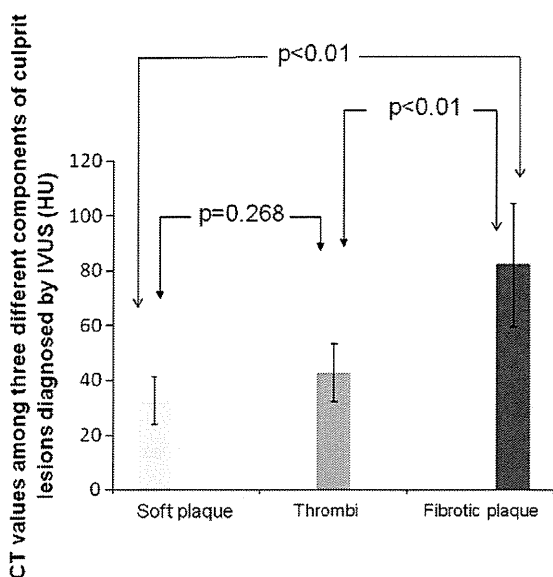
Fig. 4. Comparison of computed tomography (CT) values among three different components of culprit lesions diagnosed by intravascular ultrasound (IVUS). CT values of plaques diagnosed as soft plaques (n = 8) by IVUS were 32.9 ± 8.7 HU, which were lower than thrombi but not significantly (n = 19, 43.2 ± 10.7 HU, p = 0.268), and both of these CT values were significantly lower than those of fibrotic plaques (n = 6, 82.5 ± 22.6 HU) by IVUS (both, p<0.01).

4. Discussion

Schroeder et al. [10], reported that in subjects with stable angina pectoris, coronary arterial plaques diagnosed by IVUS could be classified by CT values as follows: 1) soft plaques would be less than 50 HU, 2) fibrous plaques would be between 50 and 119 HU and 3) calcified plaques would be more than 120 HU. Similarly, in this study, we concluded that even in ACS subjects, coronary arterial soft and fibrous plaques and also thrombi in culprit lesions of coronary arteries diagnosed by IVUS may be classifiable non-invasively on the basis of CT values.
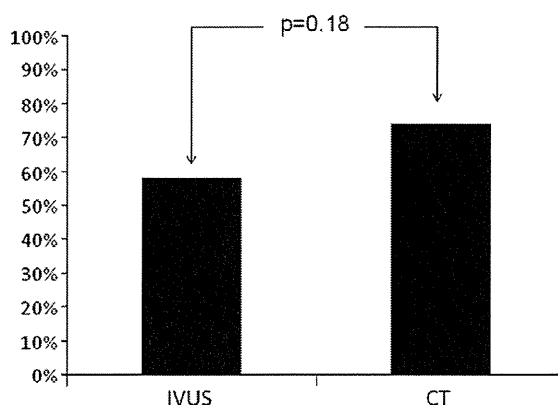

Fig. 6. Comparisons of percentage positive arterial remodeling in intravascular ultrasound (IVUS) and multislice computed tomography (CT). Positive arterial remodeling was observed in 58.1% of culprit lesions in coronary arteries by IVUS and 74.2% by CT; these percentages were not significantly different between IVUS and CT (both p = 0.18).

4.1. Characteristics of culprit lesions in ACS subjects with regard to CT values, area, calcification and positive arterial remodeling

Rupture of a vulnerable soft plaque containing a large-sized lipid core has recently been shown to precipitate ACS [16].

In this study involving IVUS, 58% of ACS subjects exhibited a thrombus estimated to be due to plaque rupture, and 19% exhibited soft plaques. However, in the remaining 23%, the main components of culprit lesions were considered to be fibrotic plaques. We speculated that plaques would usually incorporate not one, but a number of components and these might often be mixed or connected. In those subjects who exhibit fibrous plaques in culprit lesions, the lipid cores of soft plaques may adhere to the fibrotic plaque, which may then rupture, leading to the precipitation of ACS.

Inter-observer variabilities of CT values and area of plaque or thrombi in culprit lesions by two observers were excellent. However, areas of coronary arterial culprit lesions were greater on CT than IVUS. Similarly, the incidence of positive arterial remodeling tended to be greater on CT than IVUS, but this was not significant. We speculated that, in IVUS, we traced the EEM as the outer arterial border and did not detect the entire adventitial area; this would result in the area on CT
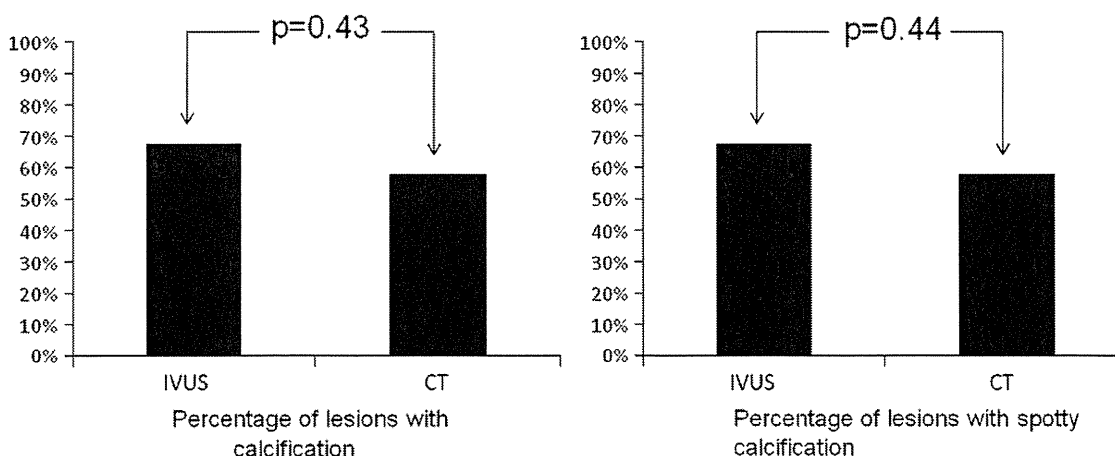

Fig. 5. Comparisons of percentage calcification and spotty calcification in culprit lesions in coronary arteries detected by intravascular ultrasound (IVUS) and multislice computed tomography (CT). Calcification was observed in 67.7% of culprit lesions in IVUS and 58.1% in CT and spotty calcification was observed in 61.3% of culprit lesions in IVUS and 51.6% in CT; these percentages were not significantly different between IVUS and CT (p = 0.43 and 0.44, respectively).
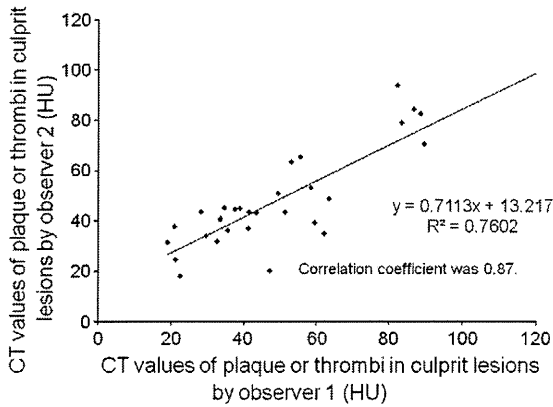
Fig. 7. Inter-observer variability between two observers of computed tomographic (CT) values of plaque or thrombi (HU) in culprit lesions. Correlation coefficient of CT values of plaque or thrombi was 0.87 between two observers.

Fig. 9. Inter-observer variability between two observers of area of plaque or thrombi (mm^2) in culprit lesions on computed tomography (CT). Correlation coefficient of area of plaque or thrombi in culprit lesions on CT was 0.86 between two observers.

being greater than the corresponding area on IVUS. Conversely in CT, we could not get clear CT images of the arterial walls as with IVUS in some cases, because of the partial volume effects due to lower spatial resolution of CT than IVUS, and artifacts due to high CT attenuation from calcification. Furthermore we could not clearly differentiate EEM from adventitia of arterial walls on MSCT, because their CT values differed only slightly.

Therefore we may have traced the outer line of the adventitia as arterial walls and overestimated the culprit vessel areas in those cases. There were few plaques in the proximal reference area; therefore the edges of the vessel lumens were clearer than culprit lesions in enhanced CT images and we could trace them easily. This may be the reason why the incidence of positive arterial remodeling was more on MSCT than on IVUS.

Recently, two studies [3,17] have shown that the proportion of positive arterial remodeling in ACS subjects was more than 80% on MSCT and less than 50% on IVUS; these results were similar to those of our study.

4.2. Utility of detection of thrombi and differentiation of thrombi from any plaques in culprit lesions in ACS subjects

The CT values of the culprit lesions diagnosed as thrombi with IVUS in ACS subjects were approximately 45 HU, and were higher than
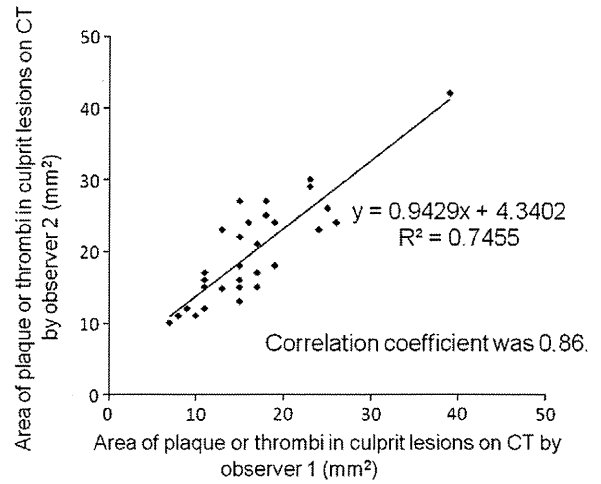
those of soft plaques (but not significantly) and significantly lower than those of fibrotic plaques. MSCT may be useful to non-invasively differentiate soft plaques or thrombi from fibrotic plaques in ACS subjects. It is very difficult to implant stents in lesions with massive thrombi, but thrombi often exist in most of the culprit lesions in ACS subjects [18]. If the presence of massive thrombi in culprit lesions could be identified in advance, without occlusion of culprit arteries on MSCT, it might be possible to administer anti-coagulation therapy for a few days and dissolve the thrombi before coronary intervention. This new strategy should allow us to implant stents in culprit lesions with fewer thrombi, and long-term patency outcomes for culprit lesions might improve after coronary intervention in ACS subjects.

The utility of drug-eluting stents has been recently established; such new stents need to be deployed with care so that they adhere closely to the internal walls of the artery, for maintenance of patency [18,19]. Therefore it would be very important to dissolve thrombi located in culprit lesions before implantation of coronary stents. These new stents have the potential to be used widely in treatment of ACS subjects from now on, and this new strategy would facilitate novel trends in coronary intervention for ACS subjects [20].
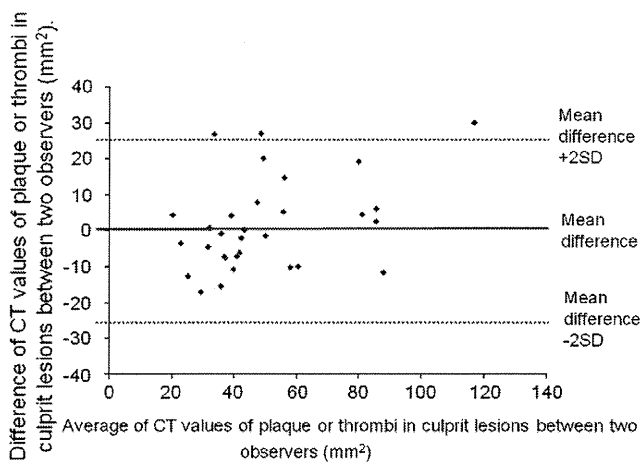

Fig. 8. Bland and Altman plot comparing computed tomographic (CT) values of plaque or thrombi in culprit lesions between two analyzers. Mean difference ± two standard deviations (SD) was 1.5 ± 25.4 HU.
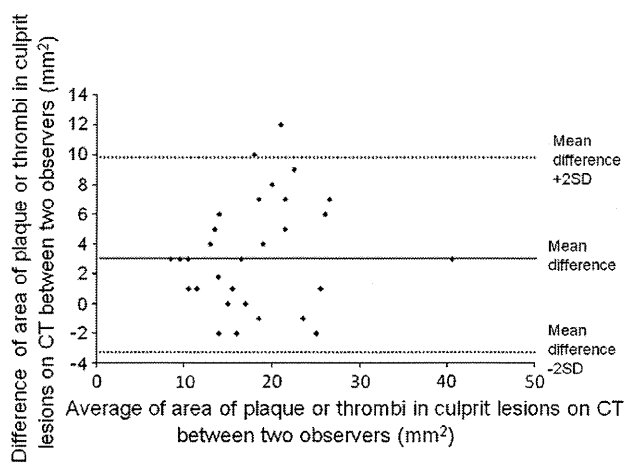

Fig. 10. Bland and Altman plot comparing area of plaque or thrombi in culprit lesions on computed tomography (CT) between two analyzers. Mean difference ± two standard deviations (SD) was 3.3 ± 6.6 mm^2.
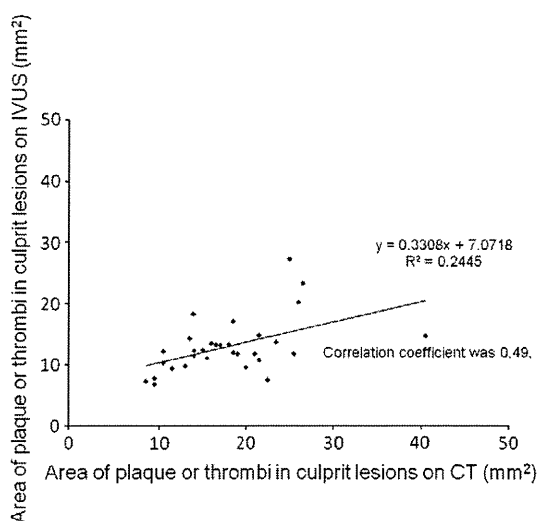
$y = 0.3308x + 7.0718$
$R^2 = 0.2445$

Correlation coefficient was 0.49.

Fig. 11. Relationship between area of plaque or thrombi (mm²) in culprit lesions on computed tomography (CT) and those on intravascular ultrasound (IVUS). The areas on CT were averages of the results from two observers. Correlation coefficient of the areas between CT and IVUS was 0.49.

4.3. Utilities of MSCT in the emergency department

The radiation exposure to MSCT for detection of coronary artery disease is 2.8–18.4 mSv [21]; we estimated that the radiation dose from 64 slice MSCT for coronary evaluation was approximately 10 mSv, while doses from coronary angiography and coronary intervention were approximately 2–3 mSv and 10–15 mSv, respectively. Such exposures cannot be discounted.

We did not routinely perform emergent coronary CT and CAG with IVUS for all patients who exhibited acute symptoms with suspicion of ACS on arrival. In our Institute, emergent coronary CT was only performed in subjects exhibiting acute symptoms with suspicion of ACS with either (1) un-interpretable ECG or (2) non diagnostic ECG or equivocal cardiac biomarker results. This is consistent with the guidelines of the American College of Cardiology Foundation Appropriate Use Criteria Task Force published in 2010 [22]. According to these criteria, subjects who have acute symptoms with suspicion of ACS are divided into three groups, namely 1) coronary heart disease

(CHD) risk low, 2) CHD risk intermediate, both of which were appropriate for CT examination, 3) CHD risk high, which was uncertain for CT examination in both (1) un-interpretable ECG, and (2) non diagnostic ECG or equivocal cardiac biomarker cases. In fact, approximately 2–8% of patients with ACS were mistakenly sent home from the emergency room, and the discharge of such patients may be associated with increased mortality, according to previous reports [23,24]. Among subjects who underwent CT in the study, many who were CHD risk low exhibited normal angiographic findings and could go home safely without performing CAG. This was because CT angiography had high negative predictive values for detecting luminal stenosis [24] (note: The original sentence above has been divided into two, for clarity). Furthermore, this is why subjects who were CHD risk low were appropriate candidates for CT examination according to American College of Cardiology Foundation Appropriate Use Criteria [22]. A randomized clinical trial showed that the use of cardiac CT among patients in the emergency Department with a normal ECG and normal initial cardiac biomarkers led to more rapid discharge and cost savings compared with a conventional serial biomarker examination [25].

Therefore we can reduce unnecessary CAG for such subjects. Indeed subjects with normal CT angiography were not included in this study. Furthermore we tried to minimize the radiation dose of coronary CT by using recently developed techniques, for example the dose modulation technique, as mentioned in Materials and methods, and also a reduced amount of contrast material in consideration of renal function. In fact, no subjects developed renal or cardiac dysfunction after these procedures.

Considering the patient characteristics indicated in Table 1, many of the subjects in this study were CHD risk intermediate, while the majoritiy of the rest were CHD risk high, thereby justifying appropriate CT examination, and some were uncertain, based upon the criteria [22].

After CT examination, we only performed CAG in subjects who gave rise to suspicion of ACS based on the results of the emergent coronary CT in which luminal stenosis was observed. If we found culprit lesions on CAG, we further performed IVUS in those responsible coronary arteries as a routine clinical procedure.

If we differentiate characteristics of plaque or thrombi in culprit lesions in coronary arteries in those subjects from information obtained non invasively by CT, as mentioned above, we may be able to plan suitable strategies for coronary intervention. This would be in addition to obtaining information about myocardium, differentiation of aortic dissection or pulmonary arterial thromboembolism, known as triple-rule-out CT.

4.4. Limitations

This was a retrospective-observational study conducted at a single tertiary medical center with small numbers of subjects.

We may not be able to detect very small degrees of calcification in MSCT because of the limit of spatial resolution of CT; therefore, while we may measure some CT values of components such as modest calcification in plaques, the measurement CT values of plaque or thrombi in culprit lesions may overestimate the true CT values.

We used the double oblique technique to make CSA images on CT. However, concerning IVUS, we did not confirm whether the transducer was parallel to the long axis of the coronary arteries and CSA images of coronary arteries perpendicular to the long axis may not have been obtained; this would influence the accuracy of measurements of plaque area or thrombi.

5. Conclusion

64-slice CT can non-invasively evaluate image characteristics in culprit lesions in coronary arteries in ACS subjects accurately as

Mean difference +2SD

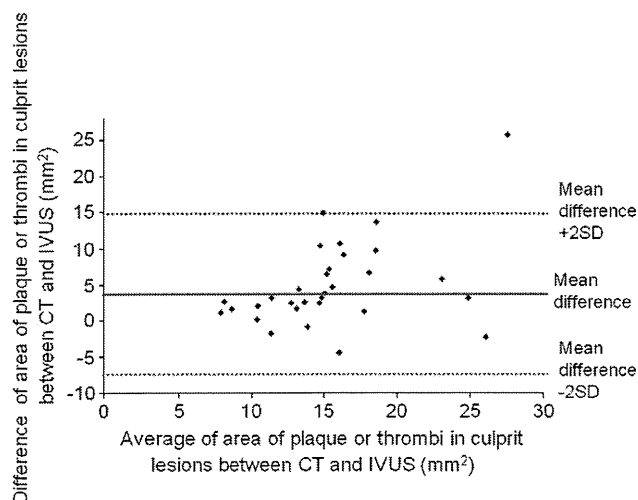Mean difference

Mean difference -2SD

Fig. 12. Bland and Altman plot comparing area of plaque or thrombi in culprit lesions on computed tomography (CT) and intravascular ultrasound. Mean difference ± two standard deviations (SD) was 4.9 ± 11.9 mm².

effectively as traditional diagnoses of IVUS. This may help to differentiate soft plaques or thrombi due to plaque rupture from fibrotic plaques.

Acknowledgment

References

[1] Yamagishi M, Terashima M, Awano K, et al. Morphology of vulnerable coronary plaque: insights from follow-up of patients examined by intravascular ultrasound before an acute coronary syndrome. J Am Coll Cardiol 2000;35:106–11.

[2] Nair A, Kuban B, Tuzeu E, et al. Coronary plaque classification with intravascular ultrasound radiofrequency data analysis. Circulation 2002;106:2200–6.

[3] Ehara S, Kobayashi Y, Yoshiyama M, et al. Spotty calcification typifies the culprit plaque in patients with acute myocardial infarction: an intravascular ultrasound study. Circulation 2004;110:3424–9.

[4] Mollet NR, Cademartiri F, Mieghem C, et al. High-resolution spiral computed tomography coronary angiography in patients referred for diagnostic conventional coronary angiography. Circulation 2005;112:2318–23.

[5] Uehara M, Funabashi N, Mikami Y, Shiina Y, Nakamura K, Komuro I. Quantitative effect of Atorvastatin on size and content of non-calcified plaques of coronary arteries one year after Atorvastatin treatment by multislice computed tomography. Int J Cardiol 2008;129:269–75.

[6] Nakamura K, Funabashi N, Uehara M, et al. Impairment factors for evaluating the patency of drug-eluting stents and bare metal stents in coronary arteries by 64-slice computed tomography versus invasive coronary angiography. Int J Cardiol 2008;130:349–56.

[7] Hori Y, Funabashi N, Uehara M, et al. Positive influence of aging on the occurrence of fat replacement in the right ventricular myocardium determined by multislice-CT in subjects with atherosclerosis. Int J Cardiol 2010;142:152–8.

[8] Ono H, Funabashi N, Uehara M, et al. Comprehensive evaluation of characteristics of left ventricular myocardium in a subject with non-coronary arterial cardiac dysfunction through segment by segment analysis using various diagnostic modalities. Int J Cardiol 2010;145:95–100.

[9] Nakamura K, Funabashi N, Uehara M, et al. Quantitative 4-dimensional volumetric analysis of left ventricle in ischemic heart disease by 64-slice computed tomography: a comparative study with invasive left ventriculogram. Int J Cardiol 2008;129:42–52.

[10] Schroeder S, Kopp AF, Baumbach A, et al. Noninvasive detection and evaluation of atherosclerotic coronary plaques with multislice computed tomography. J Am Coll Cardiol 2001;37:1430–5.

[11] Achenbach S, Moselewski F, Ropers D, et al. Detection of calcified and noncalcified coronary atherosclerotic plaque by Contrast-Enhanced, submillimeter multidetector spiral computed tomography. Circulation 2004;109:14–7.

[12] Agatston AS, Janowitz WR, Hildner FJ, et al. Quantification of coronary artery calcium using ultrafast computed tomography. J Am Coll Cardiol 1990;15:827–32.

[13] Leber AW, Knez A, White CW, et al. Composition of coronary atherosclerotic plaques in patients with acute myocardial infarction and stable angina pectoris determined by contrast-enhanced multislice computed tomography. Am J Cardiol 2003;91:714–8.

[14] Mintz GS, Nissen SE, Anderson WD, et al. American College of Cardiology Clinical Expert Consensus Document on Standards for Acquisition, Measurement and Reporting of Intravascular Ultrasound Studies (IVUS). A report of the American College of Cardiology Task Force on Clinical Expert Consensus Documents. J Am Coll Cardiol 2001;37:1478–92.

[15] Barger AC, Beeuwkes III R. Rupture of coronary vasa vasorum as a trigger of acute myocardial infarction. Am J Cardiol 1990;66:41G–3G.

[16] Fuster V, Stein B, Ambrose JA, et al. Atherosclerotic plaque rupture and thrombosis. Evolving concepts. Circulation 1990;82:II47–59.

[17] Motoyama S, Kondo T, Sarai M, et al. Multislice computed tomographic characteristics of coronary lesions in acute coronary syndromes. J Am Coll Cardiol 2007;50:319–26.

[18] Mizuno K, Satomura K, Miyamoto A, et al. Angioscopic evaluation of coronary-artery thrombi in acute coronary syndromes. N Engl J Med 1992;326:287–91.

[19] Fujii K, Carlier SG, Mintz GS, et al. Stent underexpansion and residual reference segment stenosis are related to stent thrombosis after sirolimus-eluting stent implantation: an intravascular ultrasound study. J Am Coll Cardiol 2005;45:995–8.

[20] Nomoto K, Watanabe I, Oba T, et al. Safety and efficacy of sirolimus-eluting stent in patients with acute coronary syndrome undergoing emergency procedure. Circ J 2008;72:1054–8.

[21] Earls JP, Berman EL, Urban BA, et al. Prospectively gated transverse coronary CT angiography versus retrospectively gated helical technique: improved image quality and reduced radiation dose. Radiology 2008;246:742–53.

[22] Taylor AJ, Cerqueira M, Hodgson JM, et al. ACCF/SCCT/ACR/AHA/ASE/ASNC/NASCI/SCAI/SCMR 2010 appropriate use criteria for cardiac computed tomography: a report of the American College of Cardiology Foundation Appropriate Use Criteria Task Force, the Society of Cardiovascular Computed Tomography, the American College of Radiology, the American Heart Association, the American Society of Echocardiography, the American Society of Nuclear Cardiology, the North American Society for Cardiovascular Imaging, the Society for Cardiovascular Angiography and Interventions, and the Society for Cardiovascular Magnetic Resonance. J Am Coll Cardiol 2010;56:1864–94.

[23] Pope JH, Aufderheide TP, Ruthazer R, et al. Missed diagnoses of acute cardiac ischemia in the emergency department. N Engl J Med 2000;342:1163–70.

[24] Hoffmann U, Nagurney JT, Moselewski F, et al. Coronary multidetector computed tomography in the assessment of patients with acute chest pain. Circulation 2006;114:2251–60.

[25] Goldstein JA, Gallagher MJ, O'Neill WW, Ross MA, O'Neil BJ, Raff GL. A randomized controlled trial of multi-slice coronary computed tomography for evaluation of acute chest pain. J Am Coll Cardiol 2007;49:863–71.

[26] Shewan LG, Coats AJ. Ethics in the authorship and publishing of scientific articles. Int J Cardiol 2010;144:1–2.

CLINICAL RESEARCH

Ca^{2+} entry mode of Na$^+$/Ca^{2+} exchanger as a new therapeutic target for heart failure with preserved ejection fraction

Daisuke Kamimura[1,2,3†], Tomohito Ohtani[1†], Yasushi Sakata[1], Toshiaki Mano[1,2], Yasuharu Takeda[1,2], Shunsuke Tamaki[1,2,4], Yosuke Omori[1,2], Yasumasa Tsukamoto[1,2], Kazuharu Furutani[4,5], Yutaka Komiyama[6], Masamichi Yoshika[6], Hakuo Takahashi[6], Toshio Matsuda[7], Akemichi Baba[7], Satoshi Umemura[3], Takeshi Miwa[2], Issei Komuro[1], and Kazuhiro Yamamoto[1,4*]

[1]Department of Cardiovascular Medicine, Osaka University Graduate School of Medicine, Suita, Japan; [2]Genome Information Research Center, Osaka University, Suita, Japan; [3]Department of Medical Science and Cardiorenal Medicine, Yokohama City University Graduate School of Medicine, Yokohama, Japan; [4]The Center for Advanced Medical Engineering and Informatics, Osaka University, 2-2 Yamadaoka, 565-0871 Suita, Japan; [5]Department of Pharmacology, Osaka University Graduate School of Medicine, Suita, Japan; [6]Department of Clinical Sciences and Laboratory Medicine, Kansai Medical University, Moriguchi, Japan; and [7]Laboratory of Medicinal Pharmacology, Osaka University Graduate School of Pharmaceutical Sciences, Suita, Japan

Aims	Left ventricular (LV) fibrosis and stiffening play crucial roles in the development of heart failure with preserved ejection fraction (HFPEF). Plasma level of digitalis-like factors (DLFs) is increased in patients with hypertension, a principal underlying cardiovascular disease of HFPEF. Digitalis-like factors inhibit ion-pumping function of Na$^+$/K$^+$-ATPase and activate the Ca^{2+} entry mode of Na$^+$/Ca^{2+} exchanger (NCX). Digitalis-like factors are known to promote collagen production in fibroblasts. The aim of this study was to explore whether the pharmacological inhibition of the NCX entry mode is effective in the prevention of LV fibrosis and in the development of HFPEF.
Methods and results	(i) Dahl salt-sensitive rats fed 8% NaCl diet from age 6 weeks served as hypertensive HFPEF model. In this model, 24 h urine excretion of DLFs was greater than that in the age-matched control at compensatory hypertrophic and heart failure stages. (ii) Continuous administration of ouabain for 14 weeks developed LV fibrosis without affecting blood pressure in Sprague–Dawley rats. (iii) Ouabain elevated intracellular Ca^{2+} concentration through the entry of extracellular Ca^{2+}, increased the phosphorylation level of p42/44 mitogen-activated protein kinases, and enhanced ^{3}H-proline incorporation in cardiac fibroblast; and SEA0400, the inhibitor of the NCX entry mode, suppressed these effects. (iv) In the HFPEF model, administration of SEA0400 at subdepressor dose improved the survival rate in association with the attenuation of LV fibrosis and stiffening.
Conclusion	Digitalis-like factors and the subsequently activated NCX entry mode may play an important role in the development of hypertensive HFPEF, and the blockade of the NCX entry mode may be a new therapeutic strategy for this phenotype of heart failure.
Keywords	Heart failure • Diastole • Fibrosis • Na$^+$/Ca^{2+} exchanger • Digitalis-like factors

Introduction

Heart failure with preserved ejection fraction (HFPEF) has poor prognosis and its prevalence has increased over the past two decades.[1] In spite of its socioeconomic burden, therapeutic strategy has not been established. The progression of left ventricular (LV) stiffening plays a crucial role in the transition from asymptomatic LV hypertrophy to HFPEF[2] and is attributed to myocardial fibrosis.[3] Thus, LV fibrosis is likely a therapeutic target for HFPEF.

* Corresponding author. Tel: +81 6 6879 6612, Fax: +81 6 879 6613, Email: kazuhiro@medone.med.osaka-u.ac.jp

Digitalis-like factors (DLFs), such as ouabain and marinobufagenin, exist in humans. The elevation of plasma level of ouabain was observed in patients with hypertension,[4] a principal underlying cardiovascular disease of HFPEF.[1] Digitalis-like factors promote collagen production in fibroblasts, and the activation of p42/44 mitogen-activated protein kinases (MAPKs) plays an important role in collagen synthesis.[5,6] Previous in vitro studies have reported the DLFs-induced activation of Src-p42/44 MAPKs pathway through non-pumping function of Na^+/K^+-ATPase signalosome.[5,7] However, the binding of DLFs to Na^+/K^+-ATPase also leads to the inactivation of its ion-pumping function, and the Na^+-lag hypothesis assumes that this process increases intracellular Na^+ concentration and subsequently raises intracellular Ca^{2+} concentration ($[Ca^{2+}]_i$) through the change in the mode of Na^+/Ca^{2+} exchanger (NCX) from Ca^{2+} exit (forward) to entry (reverse) mode.[8] Kometiani et al.[9] demonstrated that the increase in $[Ca^{2+}]_i$ leads to the activation of p42/44 MAPKs in myocytes, although another study showed contradictory results.[10] The relation among these factors is unknown in fibroblast.

We hypothesized that DLFs are one of risk factors for the development of HFPEF, and this study aimed at exploring whether the pharmacological inhibition of the Ca^{2+} entry mode of NCX is effective in preventing the development of LV fibrosis and the transition to hypertensive HFPEF.

Methods

This study consists of following in vivo and in vitro studies, and details are provided in the supplementary data.

Study 1: Urinary excretion of DLFs in the HFPEF model.
Study 2: Effects of ouabain on cardiac structure.
Study 3: Effects of ouabain and the NCX inhibitor on cardiac fibroblast.
Study 4: Effects of NCX inhibitor on the HFPEF model.

Results

Study 1: Urinary excretion of digitalis-like factors in the HFPEF model rats

At the age of 19 weeks of the HFPEF model, the ratio of LV mass to tibial length and the ratio of lung weight to tibial length were increased without the decrease in LV endocardial or mid-wall fractional shortening or the changes in LV end-diastolic dimension (Table 1). Thus, the HFPEF model of this study protocol represented the characteristics of the hypertensive HFPEF model as published in the previous studies.[2,11] Urinary excretion of ouabain-like immunoreactivity was significantly higher in the HFPEF model than in the age-matched control at the age of 13 and 19 weeks (Figure 1A). Urinary excretion of marinobufagenin-like immunoreactivity also increased at the age of 13 weeks and tended to be high at the age of 19 weeks in the HFPEF model rats when compared with the age-matched control (Figure 1B).

Study 2: Effects of ouabain on cardiac structure in Sprague–Dawley rats

There was no significant difference in systolic blood pressure, echocardiographic parameters, or a ratio of LV mass to tibial

Table 1 Echocardiographic and pathological parameters at the age of 19 weeks in Study 1 (Dahl salt-sensitive rats)

	Control (n = 6)	HFPEF model (n = 6)	P-value
Systolic blood pressure (mmHg)	129 ± 3	232 ± 13*	<0.001
LV end-diastolic dimension (mm)	9.3 ± 0.2	9.0 ± 1.0	0.459
LV posterior wall thickness at end-diastole (mm)	1.2 ± 0.1	1.7 ± 0.1*	0.003
LV endocardial fractional shortening (%)	28 ± 2	27 ± 4	0.482
LV mid-wall fractional shortening (%)	17 ± 1	15 ± 3	0.078
A ratio of LV mass to tibial length (mg/mm)	20 ± 1	31 ± 2*	<0.001
A ratio of lung weight to tibial length (mg/mm)	35 ± 2	53 ± 17*	0.004

Values are expressed as mean ± SD.
HFPEF, heart failure with preserved ejection fraction; LV, left ventricular.
*P < 0.05 vs. control group.

length between the ouabain and the control groups; however, LV area of fibrosis was significantly greater in the ouabain group than in the control group irrespective of NaCl concentration of chow (Table 2, Figure 2).

Study 3: Effects of ouabain and SEA0400 on cardiac fibroblast

Intracellular Ca^{2+} dynamics

In normal physiologic saline solution (PSS) (control), the fibroblasts responded to bath-applied ouabain with robust Ca^{2+} transient (Figure 3A and D). This Ca^{2+} signal was completely diminished by removal of Ca^{2+} from extracellular PSS (Figure 3B and D). Furthermore, SEA0400, an NCX inhibitor that preferentially blocks the Ca^{2+} entry mode,[12] substantially suppressed the ouabain-induced elevation of $[Ca^{2+}]_i$ (Figure 3C and D). In quite contrast, Ca^{2+} release stimulated by angiotensin II normally occurred in the absence of extracellular Ca^{2+}, or in the presence of SEA0400 (Figure 3A–C). These results suggest that the ouabain-induced elevation of $[Ca^{2+}]_i$ is largely attributed to the Ca^{2+} entry mode operation of the NCX.

^{3}H-proline incorporation and p42/44 mitogen-activated protein kinase activity

^{3}H-proline incorporation (Figure 4A) and the phosphorylation of p42/44 MAPK (Figure 4B) were promoted by ouabain administration in cardiac fibroblasts. SEA0400 suppressed these effects of ouabain, but did not affect the baseline levels.
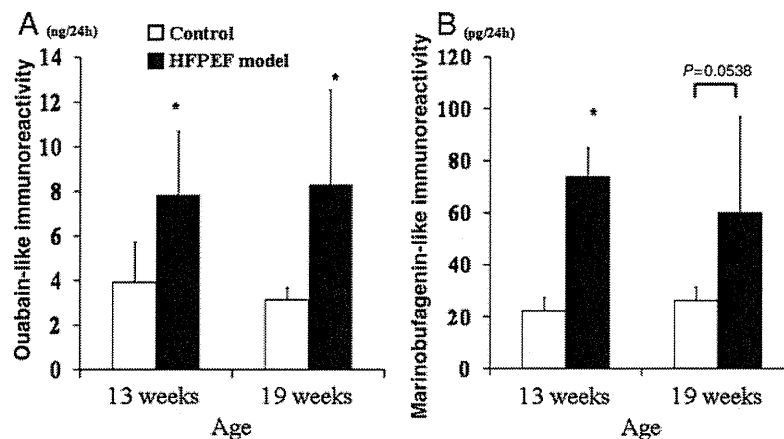
Figure 1 The 24 h urinary excretion of ouabain-like immunoreactivity (A) and marinobufagenin-like immunoreactivity (B) at the age of 13 and 19 weeks in the control and HFPEF model. Data are presented as mean ± SD. *P < 0.05 vs. control.

Table 2 Haemodynamic and echocardiographic parameters at the age of 20 weeks in Study 2 (Sprague–Dawley rats)

	Low-salt diet			High-salt diet		
	Control (n = 4)	Ouabain (n = 6)	P-value	Control (n = 4)	Ouabain (n = 6)	P-value
Systolic blood pressure (mmHg)	128 ± 7	130 ± 1	0.959	130 ± 7	129 ± 11	0.818
LV end-diastolic dimension (mm)	8.5 ± 0.5	9.0 ± 0.3	0.077	9.5 ± 0.3	9.2 ± 0.3	0.150
LV posterior wall thickness at end-diastole (mm)	1.4 ± 0.2	1.4 ± 0.1	0.915	1.5 ± 0.1	1.6 ± 0.1	0.176
LV endocardial fractional shortening (%)	38 ± 6	35 ± 2	0.286	39 ± 6	36 ± 3	0.345
LV mid-wall fractional shortening (%)	21 ± 4	19 ± 1	0.333	21 ± 2	20 ± 2	0.322
E/A ratio	1.9 ± 0.4	1.9 ± 0.8	0.999	1.6 ± 0.3	1.5 ± 0.1	0.412
Deceleration time of mitral E-wave (ms)	46 ± 6	45 ± 4	0.700	53 ± 6	55 ± 4	0.459

Values are expressed as mean ± SD.
E/A ratio, a ratio of peak early diastolic filling velocity to peak filling velocity at atrial contraction.

Study 4: Effects of Na$^+$/Ca^{2+} exchanger inhibitor on HFPEF model rats

Survival study

The administration of SEA0400 improved the survival rate of the HFPEF model (Figure 5A). All of the rats of the untreated group which died during the protocol were associated with pulmonary congestion. There were no differences in systolic blood pressure (P = 0.056–0.801) or heart rate (P = 0.091–0.689) between two groups at any age (Figure 5B and C).

Haemodynamic and pathophysiological study

Before data collection, 5 of 14 rats in the untreated group and 2 of 12 rats in the SEA group died with pulmonary congestion. We could not collect data in one rat of the untreated group and two rats of the SEA group because of technical failure in the process of cardiac catheterization. Therefore, data from eight rats in the untreated group, eight rats in the SEA group, and eight rats in

the control group were analysed. All echocardiographic and haemodynamic data are summarized in Table 3. Systolic blood pressure, heart rate, LV mid-wall fractional shortening, LV end-diastolic dimension, the ratio of LV mass to tibial length, and the time constant of LV relaxation were not different between the untreated group and the SEA group. However, myocardial stiffness constant, LV end-diastolic pressure, and the ratio of lung weight to tibial length were significantly lower in the SEA group than in the untreated group.

The area of LV fibrosis was greater in the untreated group than in the control group (Figure 6). The mRNA level of type I collagen was increased by 5.7-fold (P < 0.05), and the hydroxyproline content of LV myocardium was higher in the untreated group than in the control group (4.6 ± 0.7 vs. 3.3 ± 0.5 μmol/g, P < 0.05). The administration of SEA0400 reduced the area of LV fibrosis (Figure 6) in association with the significant decrease in type I collagen mRNA level by 21% (P < 0.05). Left ventricular hydroxyproline content in the SEA group (4.2 ± 0.4 μmol/g) tended to be
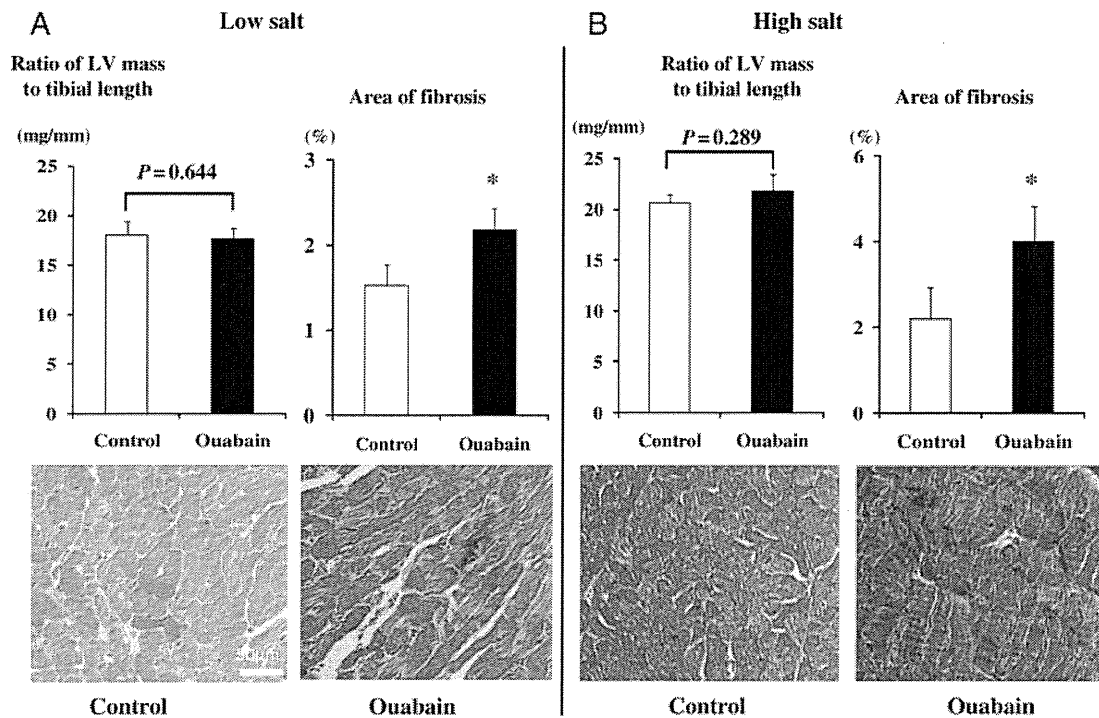
Figure 2 Post-mortem ratio of left ventricular mass to tibial length and area of left ventricular fibrosis in Sprague–Dawley rats with and without the administration of ouabain under low-salt (A) and high-salt (B) diet. The representative photomicrographs of Azan Mallory staining of the left ventricle are shown below. Data are presented as mean ± SD. *P < 0.05 vs. control.

decreased when compared with the untreated group, although the difference was not statistically significant. The activity of 72 kDa gelatinase (matrix metalloproteinase-2) was significantly enhanced in the untreated group compared with the control group and was attenuated in the SEA group (Figure 7).

Discussion

The principal findings of the present study are (i) daily urinary excretion of DLFs was increased at compensated hypertrophic and heart failure stages in the HFPEF model, (ii) chronic administration of ouabain promoted cardiac fibrosis without the elevation of blood pressure irrespective of NaCl loading, (iii) ouabain elevated $[Ca^{2+}]_i$ through the entry of extracellular Ca^{2+}, and enhanced collagen production with the activation of p42/44 MAPK in cardiac fibroblast, (iv) SEA0400 suppressed these in vitro effects of ouabain, (v) SEA0400 attenuated LV fibrosis and stiffening without the antihypertensive effects and prevented pulmonary congestion and the increase in LV filling pressure in the hypertensive HFPEF model rats, leading to the improvement of survival rate.

The prevalence of HFPEF has increased, and its prognosis has not improved during the past two decades.[1] Experimental and clinical studies have shown that LV fibrosis plays a crucial role in the development of HFPEF,[2,3,13] indicating that LV fibrosis is a therapeutic target for this phenotype of heart failure. Although experimental and small-sized clinical studies have suggested the efficiency of angiotensin receptor blocker or angiotensin-converting

enzyme-inhibitor in the prevention of LV fibrosis and/or HFPEF,[11,14,15] clinical trials have failed to show the reduction of the primary outcome by these drugs.[16,17] Thus, another target to prevent fibrosis is awaited to improve the prognosis of HFPEF.

Digitalis-like factors bind to Na^+/K^+-ATPase and subsequently result in the change of the mode of NCX and the increase in $[Ca^{2+}]_i$.[8] Previous experimental studies have shown that DLFs activate MAPKs and promote collagen production in fibroblasts.[5,7] Plasma level of DLFs is elevated in a half of patients with hypertension[4] and also increases in association with the reduction of ejection fraction[18] or physical stress situations.[19,20] This study showed that the urinary excretion of DLFs was augmented in the hypertensive HFPEF model at compensatory hypertrophic and heart failure stages, which suggests the enhanced secretion of DLFs and the elevation of their plasma level in HFPEF.[21] A close relation between DLFs and the elevation of blood pressure has been reported,[7,22] but the current study demonstrated that ouabain induced collagen synthesis in vitro and promoted LV fibrosis in vivo without the induction of hypertension. The dose of ouabain in our in vitro study, Study 3, was likely above the physiological range, considering its plasma concentration.[4] This dose was chosen on the basis of the previous studies[5,23] to clarify the effects of ouabain without loss of viability and those of SEA0400 on ouabain-induced phenomenon. The dose of exogenous ouabain in our in vivo study, Study 2, was determined on the basis of the previous study,[24] and its tissue or plasma concentration was not assessed in this study. Although this study may not